ISTANBUL TECHNICAL UNIVERSITY ★ GRADUATE SCHOOL

A COMPARATIVE ANALYSIS OF mTRL AND 2X-THRU DE-EMBEDDING METHODS

M.Sc. THESIS

Tuğçe AYRAÇ

Department of Electronics and Communication Engineering

Electronics Engineering Programme

JANUARY 2024

ISTANBUL TECHNICAL UNIVERSITY ★ GRADUATE SCHOOL

A COMPARATIVE ANALYSIS OF mTRL AND 2X-THRU DE-EMBEDDING METHODS

M.Sc. THESIS

Tuğçe AYRAÇ
(504201258)

Department of Electronics and Communication Engineering

Electronics Engineering Programme

Thesis Advisor: Assoc. Prof. Metin Yazgı

JANUARY 2024

İSTANBUL TEKNİK ÜNİVERSİTESİ ★ LİSANSÜSTÜ EĞİTİM ENSTİTÜSÜ

mTRL ve 2X-THRU DE-EMBEDDING YÖNTEMLERİNİN KARŞILAŞTIRMALI ANALİZİ

YÜKSEK LİSANS TEZİ

Tuğçe AYRAÇ
(504201258)

Elektronik ve Haberleşme Mühendisliği Anabilim Dalı

Elektronik Mühendisliği Programı

Tez Danışmanı: Doç. Dr. Metin Yazgı

OCAK 2024

Tuğçe AYRAÇ, a M.Sc. student of ITU Graduate School student ID 504201258 successfully defended the thesis entitled “A COMPARATIVE ANALYSIS OF mTRL AND 2X-THRU DE-EMBEDDING METHODS”, which she prepared after fulfilling the requirements specified in the associated legislations, before the jury whose signatures are below.

Thesis Advisor :	**Assoc. Prof. Metin Yazgı** Istanbul Technical University	....
Jury Members :	**Dr. Kemal Ozanoğlu** Boğaziçi University	....
	Assoc. Prof. Onur Ferhanoğlu Istanbul Technical University	....

Date of Submission : **5 Jan 2024**
Date of Defense : **6 Feb 2024**

To my loyal friend, forever in the light..

FOREWORD

I would like to express my sincere appreciation to both my thesis advisor, Assoc. Prof. Metin Yazgı, and my co-advisor, Dr. Kemal Ozanoğlu, for their invaluable guidance throughout this thesis.

I would like to thank Assoc. Prof. Onur Ferhanoğlu for attending my thesis defense.

A special acknowledgment is extended to Mikroelektronik Ltd. (MKR-IC) for their support and resources, which played a crucial role in the completion of this thesis. I wish to extend my deepest gratitude to Emre Apaydın for his exceptional support throughout the completion of this thesis.

Finally and most importantly, I would like to thank my family, they always supported me through tough times and believe in me to achieve success.

January 2024 Tuğçe AYRAÇ

TABLE OF CONTENTS

ABBREVIATIONS

VNA	: Vector Network Analyzer
BDK	: Baskı Devre Kartı
PCB	: Printed Circuit Board
DUT	: Device Under Test
TDR	: Time Domain Reflectometer
FDF	: Fixture DUT Fixture
ZC	: Impedance Correction
NZC	: Non-Impedance Correction
VSWR	: Voltage Standing Wave Ratio
GSG	: Ground Signal Ground
COB	: Chip on Board
IC	: Integrated Circuit
E-Cal	: Electronic Calibration
mTRL	: Multiline Thru-Reflect-Line
GHz	: Giga Hertz
dB	: Decibel

SYMBOLS

γ	: Propagation Constant
ε_{eff}	: Effective Permittivity
f	: Frequency
ϕ_{eff}	: Effective Phase Difference
Φ	: Relative Phase Offset
c	: Speed of Light
ε_r	: Effective Dielectric Constant

LIST OF TABLES

LIST OF FIGURES

A COMPARATIVE ANALYSIS OF mTRL AND 2X-THRU DE-EMBEDDING METHODS

SUMMARY

In high-frequency measurements, accurate characterization faces challenges arising from parasitic effects introduced by the measurement setup. These effects, which include artifacts from test fixtures, cables and connectors, can significantly impact the precision of measurements. The standard method for S-parameter characterization performed by a Vector Network Analyzer (VNA) in the frequency domain. Typically, a Device Under Test (DUT) is mounted on a Printed Circuit Board (PCB) to establish a connection with the VNA. It is crucial to eliminate any artifacts introduced by the test fixture to obtain the actual performance of the DUT. The de-embedding process aims to eliminate these parasitic effects and reveal the intrinsic electrical properties of the DUT.

This study comprehensively analyzes two distinct de-embedding techniques: the Multiline Thru-Reflect-Line (mTRL) method and the 2X-Thru fixture removal. The methods are compared regarding calibration standard requirements, de-embedding methodology, fixture removing accuracy, and de-embedding results. The comparison reveals that the accuracy of the mTRL method strictly depends on the impedance variation between calibration standards. Conversely, the 2X-Thru with impedance correction, on the other hand, is more susceptible to impedance variation since it relies on a single calibration standard, which also eases the measurement routine and reduces the complexity. Self-test fixture de-embedding was performed for both calibration methods to validate the calibrations, with subsequent checks on the transmission coefficients of residuals. In both calibration methods, the de-embedding results of DUT were compared by evaluating transmission reflection coefficient parameters and the TDR responses of the de-embedded structure. The calibration was verified using the test structure recommended by the *IEEE P370 Electrical Characterization of Printed Circuit Board and Related Interconnects at Frequencies up to 50 GHz* standard, and the fabrication tolerances of the implemented de-embedding structures were evaluated.

One important aim of this study is to contribute to the development of open-source de-embedding tools since the validity and accuracy of commercial tools cannot be thoroughly evaluated for academic purposes. In this context, the study also shares results obtained from commercial applications.

In the IC characterization, it is essential to address the parasitic effects arising from bond wires. Beyond on-wafer measurements, a product application involves packaging, necessitating consideration of the impact of bond wires on signal integrity. In that respect, utilizing both the mTRL and 2X-Thru de-embedding methods, a GSG

bond wire model was developed. The extraction and application results of the proposed bond wire model are presented.

As a summary, this thesis provides a detailed explanation of the methodologies employed in the mTRL and 2X-Thru methods, followed by a comprehensive comparison of the de-embedded results obtained from both approaches. Furthermore, a comparison has been made between results obtained from open-source tools and those from commercial applications. Finally, a GSG bondwire model has been developed using the both mTRL and 2X-Thru de-embedding methods.

mTRL ve 2X-THRU DE-EMBEDDING YÖNTEMLERİNİN KARŞILAŞTIRMALI ANALİZİ

ÖZET

Yüksek frekanslı ölçümler, özellikle mikrodalga ve RF uygulamalarında, doğru sonuçlar elde etmek için hassas karakterizasyon gerektirir. Ancak, test düzeni, bağlantı elemanları ve kablolar gibi fiziksel bileşenlerin parazitik etkileri, ölçümleri yanıltabilir ve gerçek devre performansını maskeleyebilir. Bu nedenle, test düzeni tarafından tanıtılan bu parazitik etkileri ortadan kaldırmak, ölçüm sonuçlarının güvenilirliğini artırmak ve doğru bir karakterizasyon yapabilmek adına kritik bir adımdır. De-embedding süreci, test düzeni ve bağlantı elemanları tarafından eklenen sanal etkileri çıkartarak, ölçüm yapılan cihazın gerçek elektriksel özelliklerini çıkarmayı amaçlar. Bu sayede, elde edilen verilerin daha doğru ve güvenilir olması sağlanır.
Bu tezde, Multiline Thru-Reflect-Line (mTRL) ve 2X-Thru de-embedding metodolojileri, Python açık kaynaklı "Scikit-rf" kütüphanesi kullanılarak sistemli bir şekilde incelenmiştir. Her bir yöntemin ayrıntılı formülasyon ve uygulama detaylarına odaklanan bireysel bir incelemesi gerçekleştirilmiştir.

Test kartı tasarlanırken, hem mTRL hem de 2X-Thru de-embedding yöntemlerinin uygulanması için tüm de-embedding standartlarını içeren RO4003C™ tabanlı bir kart tasarımı gerçekleştirilmiştir. RO4003C™, yüksek frekans ölçümlerindeki performansı sebebiyle tercih edilmiştir. Ayrıca, hatlar üretici tarafından önerilen stack-up'a göre düzenlenmiş ve 50 Ohm CPW (Coplanar Waveguide) olacak şekilde tasarlanmıştır. Ölçümlerde, CPW (Coplanar Waveguide) ve mikroşerit konfigürasyonları için özel olarak tasarlanmış 2.92 mm dişi konektör kullanılmıştır. Tüm standartlar, farklı konektörlerin neden olabileceği empedans değişimini önlemek amacıyla aynı konektör çifti kullanılarak ölçülmüştür.

Performans karşılaştırması, Multiline Thru-Reflect-Line (mTRL) ve 2X-Thru yöntemleri arasında iletim ve yansıma katsayıları açısından 20 GHz'e kadar benzer sonuçlar verdiğini göstermektedir. Ancak, mTRL yöntemi, birden fazla standart kullanarak frekans aralığını genişletmesine rağmen, özellikle TDR analizinde empedans varyasyonları oluşmaktadır. Bu dalgalanmalar, kalibrasyon standartlarının üretimindeki farklılıklara ve bunlar arasındaki empedans varyasyonlarına atfedilmektedir. Öte yandan, yalnızca bir standart gerektiren 2X-Thru yöntemi, daha basit ve maliyet etkili bir alternatif sunmaktadır. Bu basitlik, de-embedding sürecini sadeleştirmenin yanı sıra doğrudan Baskı Devre Kartı (BDK) alanını azaltarak maliyetleri ve karmaşıklığı düşürmektedir.

Bu çalışmanın önemli bir hedefi, ticari araçların akademik amaçlar için tam olarak değerlendirilememesi nedeniyle, açık kaynaklı de-embedding araçlarının geliştirilmesine katkıda bulunmaktır. Tez kapsamında, Multiline TRL ve 2X-Thru de-embedding çalışmaları, RF/Mikrodalga mühendisliği alanında kullanılan, Scikit-rf adlı açık kaynaklı ve BSD lisanslı bir kütüphane olan "Scikit-rf" üzerinden elde edilmiştir. Bu kütüphane, çalışmada sunulan her iki de-embedding yöntemi için de kalibrasyon tekniklerini açık bir kaynak olarak sunmaktadır. Çalışma kapsamında, elde edilen sonuçları değerlendirmek adına açık kaynak ve ticari olarak temin edilebilen araçlar kıyaslanmıştır. Açık kaynaklı yazılım uygulaması kullanılarak elde edilen sonuçların doğruluğu ve verimliliği, lisanslı uygulamalar olan In-Situ De-embedding (ISD) ve AICC De-Embedding Utility ile karşılaştırılmıştır. Açık kaynak ve ticari araçlar ile aynı DUT üzerinden de-embeddingi sonucunda elde edilen S-parametre ve TDR sonuçları karşılaştırılmıştır. Değerlendirmelere göre açık kaynak araçların, ticari alternatiflere kıyasla benzer performans düzeylerini elde etmede başarılı olduğunu ortaya koymuştur.

Her iki kalibrasyon yöntemi için de DUT'un de-embedding sonuçları, iletim yansıma katsayısı parametreleri ve de-embedded yapıların TDR cevapları değerlendirilerek karşılaştırılmıştır. Kalibrasyon, *IEEE P370 Electrical Characterization of Printed Circuit Board and Related Interconnects at Frequencies up to 50 GHz* standardı tarafından önerilen test yapısı kullanılarak doğrulanmış ve uygulamada kullanılan de-embedding yapılarının üretim toleransları değerlendirilmiştir.

Entegre devrelerin karakterizasyonu, genellikle kırmık seviyesinde wafer üzerinden uygun probe iğneleri ile wafer üzerindeki kırmık padlerinden ölçümler alınmasıyla başlar. Ancak, test ekipmanı maliyetlerinden ve ürün seviyesinde bir karakterizasyon gerektiğinden dolayı wafer üzerinde yapılan ölçümler haricinde, gerçek dünya uygulamaları entegre devrenin ambalajlanmasını gerektirir. Kırmık ebatlarına uygun bir pakete veya kırmığın direkt olarak test/uygulama kartına teller ile bond edilmesi ile dış dünyaya bağlantı sağlanır. Karakterizasyonda, bu bond tellerinden kaynaklanan devre performansını frekansa bağlı olarak farklı seviyelerde etkileyen parazitik etkiler bulunmaktadır. Yüksek frekans ölçümlerinde, devrenin gerçek performansını değerlendirebilmek adına bu etkilerin sonuçlardan ayrıştırılması kritiktir. Bu bağlamda, Multiline (mTRL) ve 2X-Thru de-embedding yöntemlerini birleştiren bir GSG (Toprak-Sinyal-Toprak) bond tel modeli geliştirilmiştir. Bu model, özellikle bond telleri aracılığıyla kaynaklanan parazitik etkilerin frekansa bağlı olarak nasıl değiştiğini anlamak ve bu etkileri ölçüm sonuçlarından izole etmek için tasarlanmıştır. Önerilen bond tel modeli, Multiline ve 2X-Thru de-embedding yöntemlerinin bir araya getirilmesiyle geliştirilmiş ve bu yöntemlerin birleşimiyle elde edilen sonuçlar detaylı bir şekilde açıklanmıştır.

Özetle, bu tezde açık kaynak Python "Scikit-rf" kütüphanesi kullanılarak Multiline TRL ve 2X-Thru de-embedding metodolojileri incelenmiştir ve iki yönteme ait performans sonuçları karşılaştırılmıştır. Sonuçlar, mTRL'nin standartlar arasındaki üretim kaynaklı empedans varyasyonları olmasına rağmen, 20 GHz'e kadar 2X-Thru de-embedding yöntemi ile benzer performans sergilediği görülmektedir. 2X-Thru yöntemi, sadece bir standart gerektirmesi nedeniyle daha basit ve maliyet etkili bir alternatif olarak öne çıkmaktadır. İki yöntem karşılaştırmasına ek olarak, açık kaynaklı yazılım sonuçlarının muadil lisanslı araçlarla elde edilen sonuçları da paylaşılmıştır. Özellikle 2X-Thru yönteminin lisanslı araçlar ile benzer de-embedding performansı sergilediği görülmektedir. Ayrıca, mTRL ve 2X-Thru de-embedding yöntemleri kullanılarak bir GSG (Ground-Signal-Ground) bond tel modeli geliştirilmiştir. Geliştirilen modele ait uygulama sonuçları paylaşılmıştır.

1. INTRODUCTION

De-embedding is a critical process in RF/Microwave engineering, especially when working with integrated circuits on a Printed Circuit Board (PCB). The typical measurement setup involves coaxial cables, connectors, and test fixtures on PCB with the end having Device Under Test (DUT). S-parameter measurements are then taken based on the coaxial cable end. For these measurements, the calibration reference plane is established by using standard calibration methods such as Thru-Reflect-Line (TRL) or Short-Open-Load-Thru (SOLT) to remove the effects of cabling and move the calibration reference to the cable end. However, even after this calibration, there is a significant "test fixture" that needs to be removed before accessing the real terminals of the DUT. De-embedding is the process of mathematically removing fixture effects on a measured DUT. Vector Network Analyzers (VNAs) are systematically designed to accurately measure scattering parameters in high-frequency measurement of Devices Under Tests (DUTs). The interconnects, cables, connectors, PCB traces, bond wires, and IC package connect the DUT to the VNA. Artifacts that come with test fixtures introduce errors in measured data. The process of identifying and correcting these systematic errors from DUT is known as de-embedding. The precision of measured data is significantly dependent on the accuracy of that process. De-embedding is a numerical method that moves the reference plane from the cable ends of the vector network analyzer (VNA) to the start of the Device-Under-Test (DUT) by removing the test fixtures. This procedure is crucial to obtain a precise representation of *DUT* without being affected by the networks between VNA and *DUT*.

1.1 Purpose of Thesis

The primary aim of this thesis is to perform a comparative analysis of the Multiline (mTRL) and 2X-Thru de-embedding methods, offering their methodologies, applications, and results. Notably, these methods have been implemented

using open-source Python, diverging from conventional commercial applications. Furthermore, the thesis includes a comparative examination of the outcomes derived from open-source implementations and those obtained through commercial applications.
Additionally, this study contributes to the field by introducing a GSG bondwire model developed through the integration of both mTRL and 2X-Thru de-embedding methods. Bond wires crucially impact the high-frequency characterization results of integrated circuits (ICs) used in packaged or Chip-on-Board (COB) applications. In that respect one other aim of the thesis is to develop a GSG(Ground-Signal-Ground) bondwire model for de-embedding of high frequency IC characterization results.

1.2 Organization of Thesis

The thesis is organized as follows: Section II presents fundamental terms and concepts associated with VNA calibration. 2 Section III introduces the design of a test board for implementing both mTRL and 2X-Thru de-embedding methods. Sections IV and V present the theory, application, and results of the Multiline (mTRL) and 2X-Thru de-embedding methods, respectively. In Section VI, de-embedding methods are compared and the application of verification methods is shared. In Section VII, a GSG bondwire model is presented, utilizing both Multiline (mTRL) and 2X-Thru de-embedding methods, along with the results of its measurements. Finally, Section VIII overall study is summarized.

1.3 Literature Review

Thru-Reflect-Line(TRL) is one of the most accurate calibration methods when compared to other techniques. It involves the use of a *Thru*, a *Line*, and either an *Open* or *Short* as the reflect standard [2]- [3]. Despite their advantages, the method has some drawbacks including challenges for wide frequency bands, the need for additional lines consuming PCB space, increased time and resource intensity due to accurate characterization requirements, difficulties at high frequencies, and sensitivity to impedance variations between standards.
Another technique called the Multiline TRL method (mTRL) has augmented

conventional TRL by using multiple line standards to extend the frequency range without any discontinuity [4].

A recent method named 2X-Thru is now becoming an alternative to these methods since it requires only one standard [5]. The method becomes quite attractive due to reducing the required Printed Circuit Board (PCB) area, hence cost and complexity.

This study was conducted due to the lack of literature comparing the Multiline Thru-Reflect-Line (mTRL) and 2X-Thru de-embedding methods. While there are two papers [6]- [7] that compare TRL and 2X methods, no publication has directly compared the methodologies of mTRL and 2X-Thru. This study aims to examine and compare the methodologies, applications, advantages, and disadvantages of the Multiline Thru-Reflect-Line (mTRL) and 2X-Thru de-embedding methods. There are available commercial applications for both the Multiline Thru-Reflect-Line (mTRL) and 2X-Thru de-embedding methods in the literature [6,8] and [9]. This study aims to compare the results obtained using the open-source Python Scikit-rf library with those from commercial applications.

2. FUNDAMENTALS of FIXTURE DE-EMBEDDING

VNA calibration corrects measured data by removing systematic errors due to defects in the measurement system. The precision of measurements relies heavily on the precision of calibration. In that respect, this chapter provides fundamental terms and concepts associated with VNA calibration and fixture de-embedding.

2.1 Switch Term Correction for VNAs

Fig. 2.1 is a generic block diagram of two port VNA with an internal switch. The input source can be switched to Port 1 or Port 2 of the DUT. The switch also provides a 50 Ohm Z_0 termination for the output port in each direction. a_1 and a_2 are the transmitted signal, and b_1 and b_2 are reflected signals from Port 1 and Port 2, respectively.

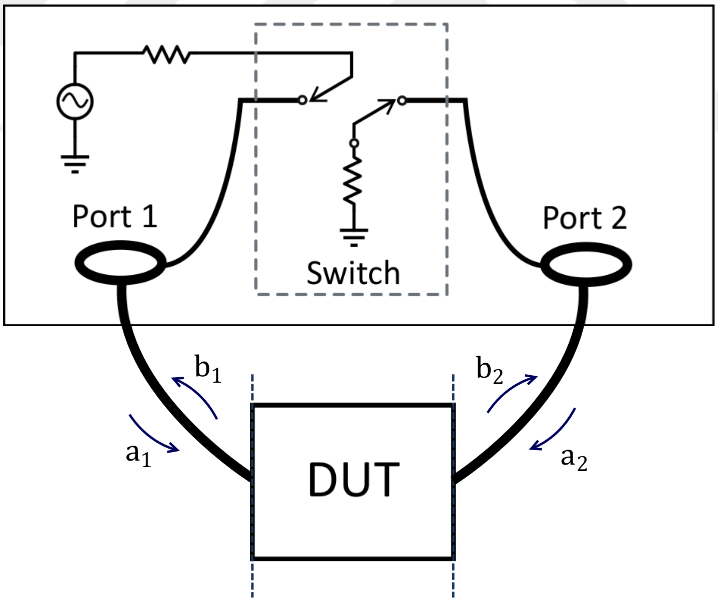

Figure 2.1 : Block diagram of two port VNA with internal switch

In the forward case, the input source is switched to port-1, and 50 Ohm termination is switched into the port-2. 50 Ohm match terminate the port-2 and $a_2 = 0$ ideally. In the forward case, reflected and transmitted waves of port-1 are described as

$$S_{11} = \left.\frac{b_1}{a_1}\right|_{a_2=0} \tag{2.1}$$

$$S_{21} = \left.\frac{b_2}{a_1}\right|_{a_2=0} \tag{2.2}$$

In the reverse case, the input source is switched to port-2, and 50 Ohm termination is switched into the port-1. 50 Ohm match terminate the port-1 and $a_1 = 0$ ideally. Reflected and transmitted waves of port-1 in the reverse case described as

$$S_{22} = \left.\frac{b_2}{a_2}\right|_{a_1=0} \tag{2.3}$$

$$S_{12} = \left.\frac{b_1}{a_2}\right|_{a_1=0} \tag{2.4}$$

The imperfect termination between ports leads to non-zero coefficients in the forward and reverse paths ($a_1 \neq 0$, $a_2 \neq 0$ and $a_1 \neq a_2$). These differences create systematic errors that need correction through a calibration algorithm.

The signal-flow representation of switch-terms in forward and reverse cases are illustrated in Fig.2.2 (a) and (b), respectively. a_{1m} and a_{2m} are the input sources for port 1 and port 2. As a result of reflections within the imperfect switch, there exists an additional signal path denoted as Γ_F, between the b_{2m} and a_{2m} nodes. Similarly, Γ_R exists for reverse direction, between the a_{1m} and b_{1m} nodes.

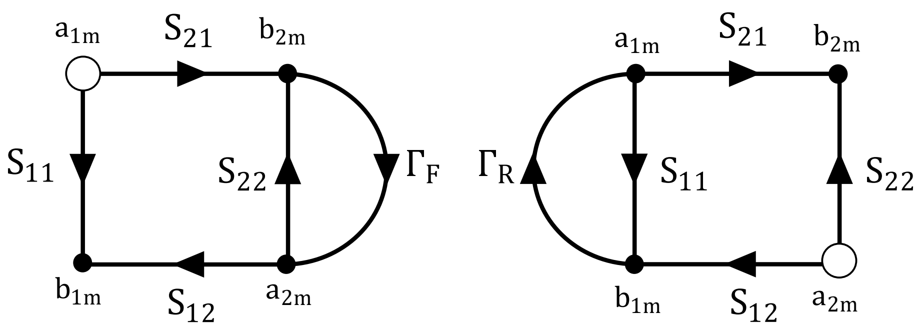

(a) (b)

Figure 2.2 : Switch term models for (a) Forward direction and (b) Reverse direction

As derivable in Fig. 2.2, also described in [10], S-parameters formulas which are free from switching errors:

$$S_{11} = \frac{S_{11}^{F} - S_{21}^{R} S_{21}^{F} \Gamma_F}{1 - S_{12}^{R} S_{21}^{F} \Gamma_R \Gamma_F} \tag{2.5}$$

$$S_{12} = \frac{S_{12}^{R} - S_{11}^{F} S_{12}^{R} \Gamma_R}{1 - S_{12}^{R} S_{21}^{F} \Gamma_R \Gamma_F} \tag{2.6}$$

$$S_{21} = \frac{S_{21}^{F} - S_{22}^{R} S_{21}^{R} \Gamma_F}{1 - S_{12}^{R} S_{21}^{F} \Gamma_R \Gamma_F} \tag{2.7}$$

$$S_{22} = \frac{S_{22}^{R} - S_{12}^{R} S_{21}^{F} \Gamma_R}{1 - S_{12}^{R} S_{21}^{F} \Gamma_R \Gamma_F} \tag{2.8}$$

2.2 Eight-Term Vector Network Analyzer Error Model

Shown in Fig. 2.3 is one of the vector network analyzer models which is described as the "Eight-Term Error Model" [10]. The Eight-Term model is derived from the "Twelwe-Term Model". Cross leakages which are from Port-1 to Port-2 and from Port-2 to Port-1, are assumed as zero and the switch is perfect. Switching between ports does not affect port match [11].

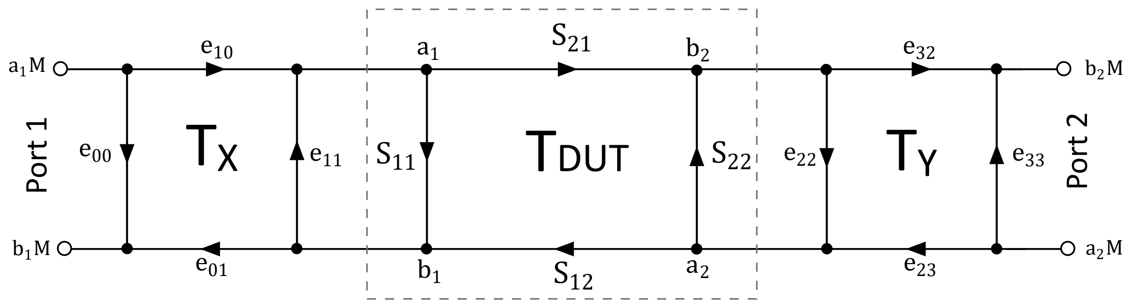

Figure 2.3 : Signal flow diagram of 8-Term Error Model for two port VNAs

Directivity, matches, reflection, and transmission terms indicated in the signal flow diagram Fig 2.3 are explained in Table 2.1.

Table 2.1 : 8-Term error model parameters of Vector Network Analyzer

Error term	Description
e_{00}, e_{33}	Directivity
e_{11}	Port 1 match
e_{22}	Port 2 match
e_{01}, e_{32}	Reflection
e_{10}, e_{23}	Transmission

T_X and T_Y are called "error boxes" and illustrate the effects of PCB trace, cables, and connectors between the VNA and measurement reference planes. System measurement of DUT with cascaded error boxes is defined as

$$T_M = T_X.T_{DUT}.T_Y \tag{2.9}$$

Cascaded matrices, T_X and T_Y, are defined as

$$T_X = \frac{1}{e^{10}} \begin{bmatrix} -\Delta_X & e^{00} \\ -e^{11} & 1 \end{bmatrix} \tag{2.10}$$

$$T_Y = \frac{1}{e^{32}} \begin{bmatrix} -\Delta_Y & e^{22} \\ -e^{33} & 1 \end{bmatrix} \tag{2.11}$$

where $\Delta_X = e_{00}e_{11} - e_{10}e_{01}$ and $\Delta_Y = e_{22}e_{33} - e_{32}e_{23}$.

From Eq. 2.10 and Eq. 2.11, scattering matrice of measured network, T_M, can be described as

$$T_M = \frac{1}{e^{10}e^{32}} \begin{bmatrix} -\Delta_X & e^{00} \\ -e^{11} & 1 \end{bmatrix} T_{DUT} \begin{bmatrix} -\Delta_Y & e^{22} \\ -e^{33} & 1 \end{bmatrix} \tag{2.12}$$

This model requires only seven parameters to analyze the two-port system.

2.3 One and Two-Tier Calibrations

Two sub-types of Vector Network Analyzer (VNA) calibration are recognized in the literature: One and Two-Tier Calibrations. One-Tier Calibration directly calibrates the entire network in a single step. In contrast, two-tier calibration involves a two-step calibration process. The first step is performed to move the reference plane to the coaxial cable end for Printed Circuit Board (PCB) measurements or a probe tip for on-wafer calibrations. With the second-tier calibration, the reference plane is shifted to the DUT. The first calibration in two-tier is a fundamental calibration step for VNAs, and it involves standard calibration procedures. This calibration helps correct systematic errors within the VNA, including the effects of the internal VNA switch. The key difference between first and second-tier calibrations is that second-tier calibration omits switch-term correction, assuming that these switch errors have been already corrected by first-tier calibration. The error boxes extracted during the second-tier calibration represent the errors introduced by only fixture and DUT.

3. DESIGN OF CALIBRATION FIXTURE

The test board designed for the implementation of both mTRL and 2X-Thru de-embedding methods is depicted in Fig. 3.1. Marked with "E" is a 10-dB attenuator, which serves as a Device Under Test (DUT). For detailed specifications of the attenuator, please refer to the datasheet [12]. The attenuator is combined with fixtures to create a "Fixture-DUT-Fixture" (FDF) unit. This unit needs to be de-embedded from its fixtures. Both fixtures are symmetrical on each side with a line length of being equal to 38.1 mm. Based on the selection of fixture length, a *Thru* which is marked as “A” was implemented as twice the length as the fixture. Both *Open* and *Short* were implemented as reflect standards for comparison, where their direct form and cascaded-with-fixture versions are marked as “B” and “C” respectively. Three lines, namely *Line1*, *Line2* (marked with “D”) and *Line3* (marked with “F”) were also implemented to provide line standards as required by the mTRL method. Their lengths with respect to *Thru* were set as Δ_{ℓ_1}=3.05 mm, Δ_{ℓ_2}=11.4 mm, and Δ_{ℓ_3}=41.1 mm respectively. Selection criteria for the required number of line standards and their corresponding lengths are detailed in Chapter 4.

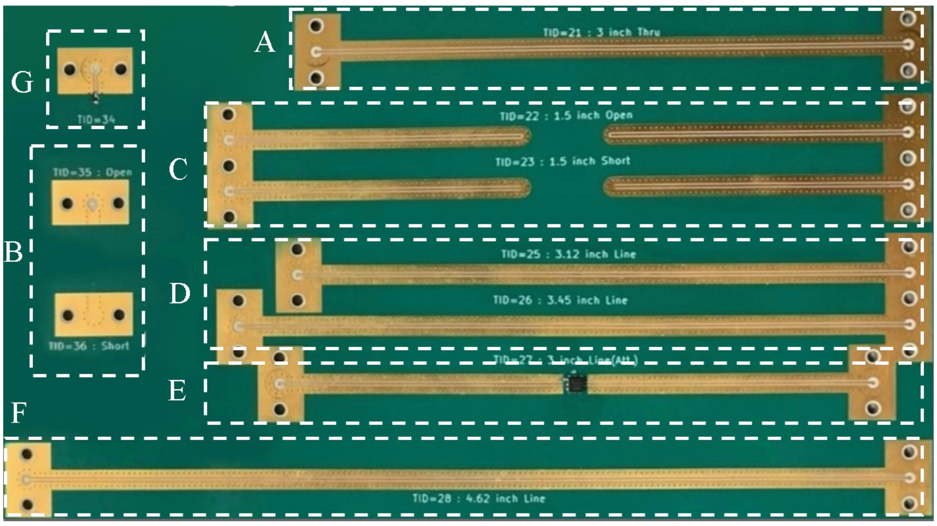

Figure 3.1 : Designed test board for mTRL and 2X-Thru de-embedding standards. Test structures are marked as: (A) *Thru*, (B) Direct *Open* and *Short*, (C) 38.1 mm *Open* and *Short*, (D) *Line1* and *Line2*, (E) *FDF*, (F) *Line3*, (G) *Load*.

Each standard was realized using a grounded coplanar waveguide (CPW) with 0.34 mm of line width and 0.13 mm of slot width on a Rogers RO4003C™ laminate with 0.2 mm of dielectric thickness. Fig. 3.2 illustrates the stack-up of the designed test board. The stack-up was designed based on the 50 Ω single-ended coplanar configuration. The core RO4003C™ materials on the top and bottom layers were adjusted according to the impedance requirements. The intermediate layer utilizes IT180A prepreg material [13], resulting in a total PCB thickness of 1.6mm.

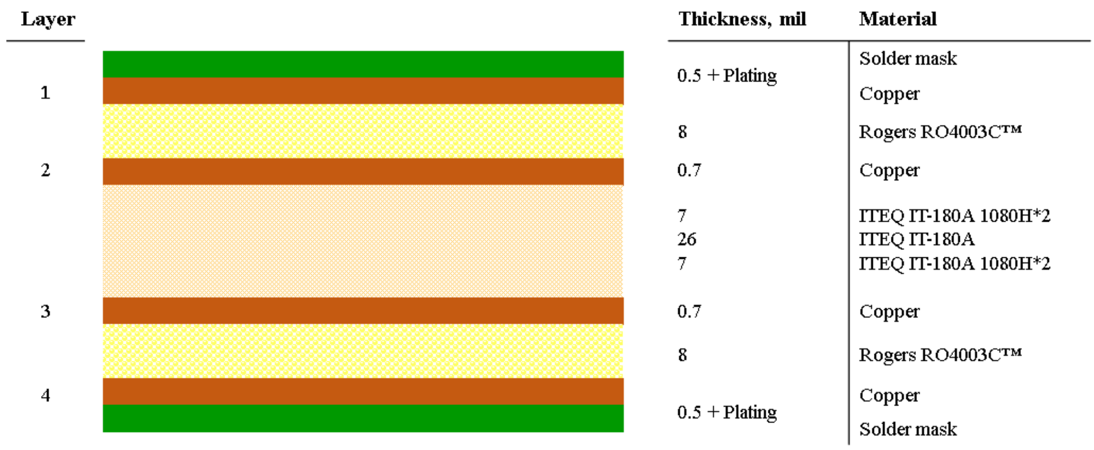

Figure 3.2 : Stack-up of the designed test board.

Before the measurement, VNA was calibrated with Keysight N7555A Electronic Calibration Module (E-Cal) [14] to set the reference plane to cable ends. In measurement, the utilized connector is a solderless 2.92 mm female compression mount connector. This connector is specifically designed for use in CPW (Coplanar Waveguide) and microstrip configurations, offering reliable performance up to 40 GHz [15]. All standards were measured using the same connector pair to prevent impedance variation introduced by different connectors. Transmission and reflection measurement results of *Thru* and *Line* standards are illustrated in Fig. 3.4. The frequency-dependent loss of the thru line with the fixture length reaches 6dB at the end of the frequency band.

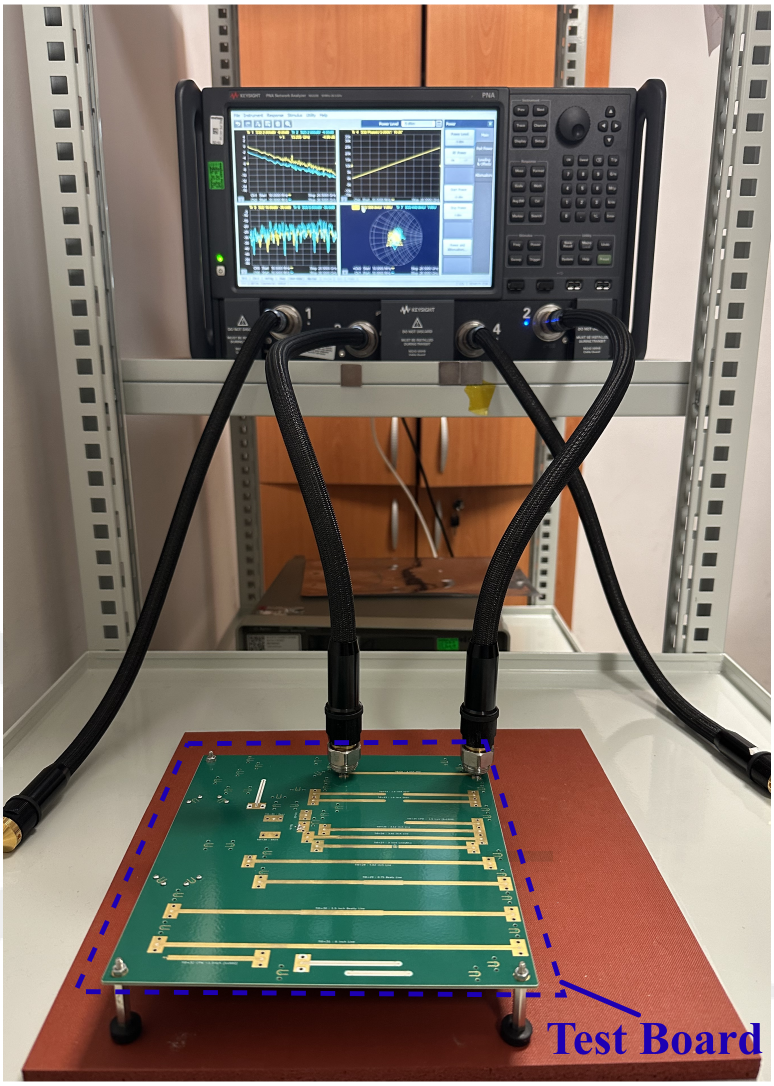

Figure 3.3 : Meaurement setup for the test board including de-embedding structures.

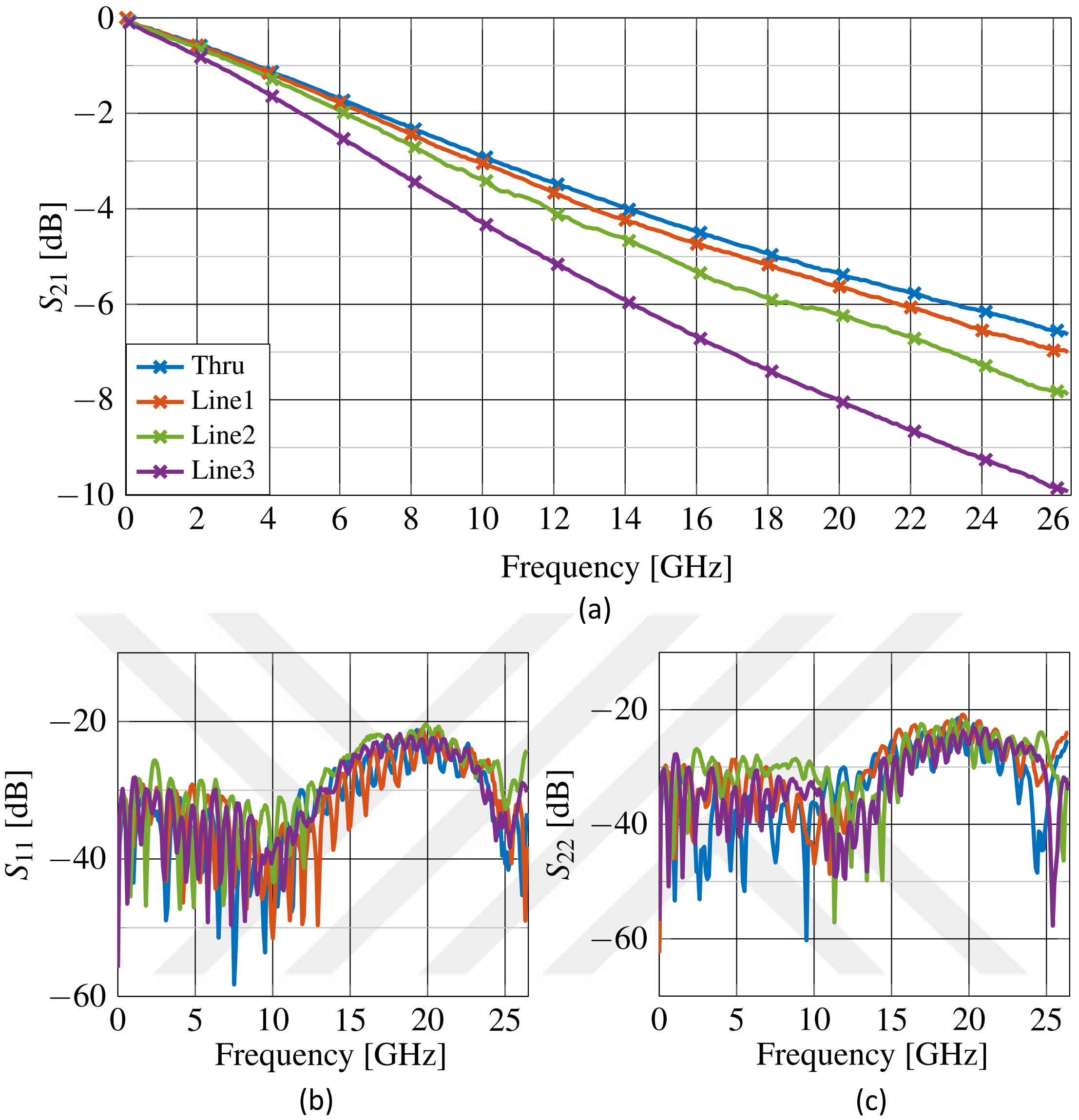

Figure 3.4 : Measurement of transmission (a) and reflection (b), (c) coefficients of *Thru* and *Line* standards.

4. mTRL DE-EMBEDDING METHOD

In this study, NIST mTRL implementation provided as an open source, BSD-licensed package for RF/Microwave engineering called “Scikit-rf” [16] has been utilized for processing mTRL calibration measurements. NIST mTRL algorithm in [16] is the one published in [17], but implementation is based on [18]. The NIST Multiline TRL algorithm use multiple lines to extend the bandwidth and accuracy of the calibration. Line standards that have different line lengths are combined to minimize the calibration error.

The required standards for the multiline TRL method are represented in Fig. 3.1. The multiline TRL algorithm requires one thru standard, a reflect standard (open or short), and line standards which have different lengths. The number of line standards is determined based on the desired bandwidth range.

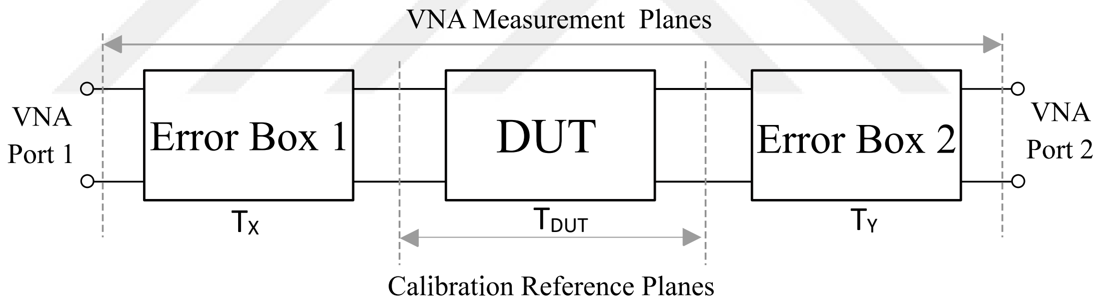

Figure 4.1 : Cascaded error boxes representing the measurement of the DUT.

As mentioned in Section 2.2, the multiline TRL calibration is based on the 8-term error box formulation as specified in Fig.4.1. DUT calibration plane and measurement planes are described. Input and output error boxes T_X and T_Y are assumed as fully symmetric. T parameter representation of measured DUT, T_M is

$$T_M = T_X T_{DUT} \overline{T_Y} \tag{4.1}$$

where T_X and T_Y are right and left error boxes of DUT. $\overline{T_Y}$ is the left-to-right error box representation of T_Y.

In the case of the multiline TRL algorithm, the T matrix of each transmission line standard is expressed as in the Eq. 4.1. Following that, T matrices of transmission line pairs are formulated as

$$T^{ij} = \begin{bmatrix} e^{-\gamma(l_j - l_i)} & 0 \\ 0 & e^{\gamma(l_j - l_i)} \end{bmatrix} \tag{4.2}$$

where l_i and l_j are the physical lengths of the i-th and j-th transmission lines, respectively, and γ is the propagation constant of the transmission lines. T_M^{ij} is the T matrix representation of measured line pairs. and T^{ij} is eigenvalue and T_X is the eigenvectors of T_M^{ij}.

In low loss or lossless cases propagation constant $\gamma = \alpha + j\beta \approx j\beta$. When the phase delay of the line is one half wavelength (180°) or its integer multiples so eigenvalue can be written as $e^{jn\pi} = \pm 1$, which n is the integer. T matrices of transmission line pairs are re-arranged as

$$T^{ij} = \begin{bmatrix} \pm 1 & 0 \\ 0 & \pm 1 \end{bmatrix} \tag{4.3}$$

Uncertainty may occur in multiples of half-wavelengths and it leads to information loss. This ill-conditioning limits the valid frequency range of the method to a certain bandwidth. However, in contrast to conventional TRL, multiline TRL uses all the lines simultaneously for each frequency point. Therefore algorithm can avoid uncertainty across the entire bandwidth.

Fig. 4.2 represents the multiline TRL de-embedding algorithm flow. If two-tier calibration has been applied, the algorithm skips the switch-term correction step. After checking of switch term correction, flow continues with computation of estimated propagation-constant γ_{est}. mTRL algorithm takes an estimated $\varepsilon_{r,eff}$, effective permittivity, for transmission line standards. γ_{est} is calculated by using user input $\varepsilon_{r,eff}$, f frequency and c speed of light:

$$\gamma_{est} = j\frac{2\pi f}{100c}\sqrt{\varepsilon'_{r,est} + j\frac{\varepsilon''_{r,est}10^9}{f}} \tag{4.4}$$

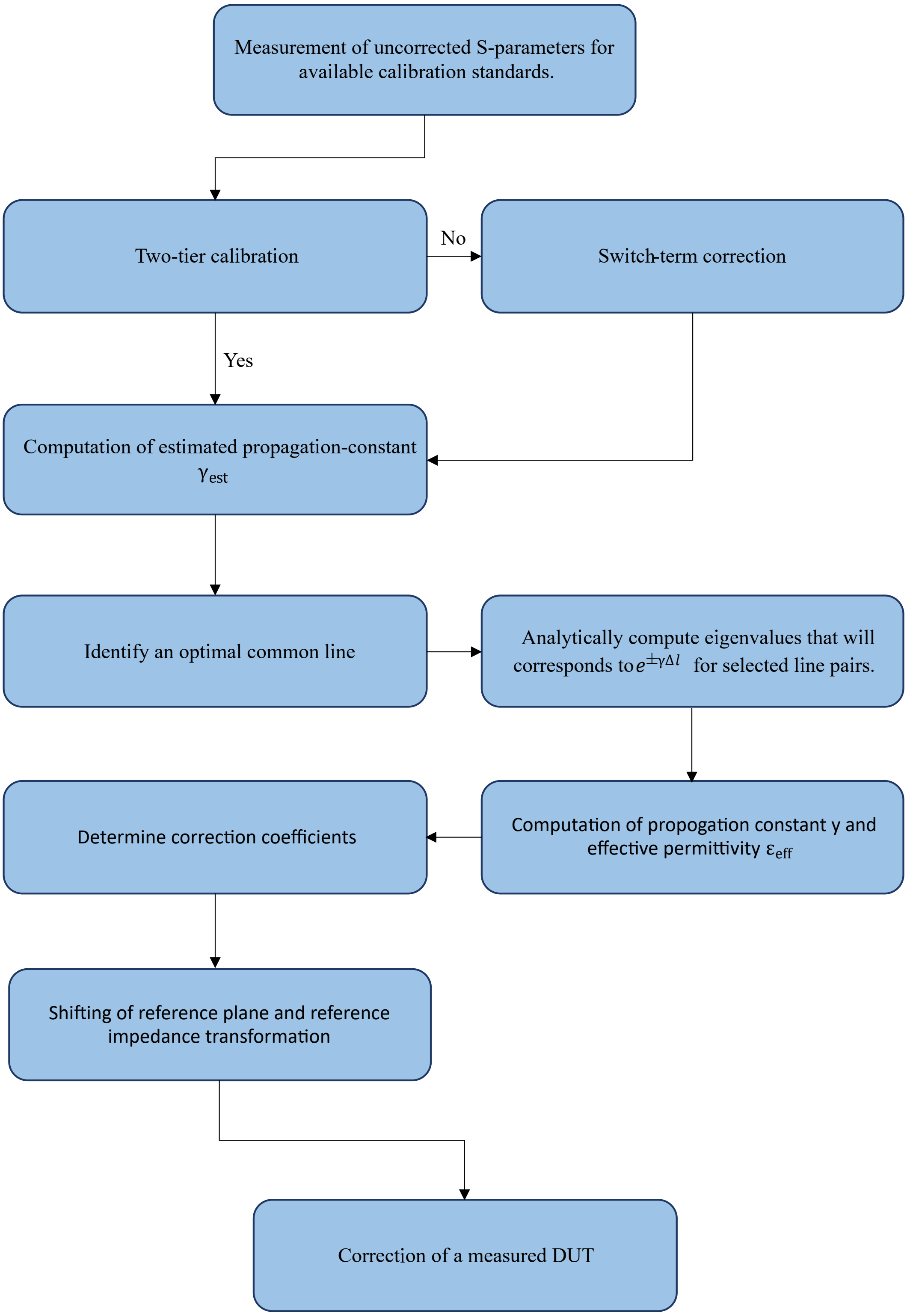

Figure 4.2 : De-embedding flow of the multiline TRL algorithm.

Eq. 4.4 is only used for the initial frequency point in the list. For the subsequent frequency points, the following formula is employed

$$\gamma_{est}(f_{n+1}) = Re\{\gamma(f_n)\} + jIm\{\gamma(f_n)\}\frac{f_{n+1}}{f_n} \tag{4.5}$$

f_{n+1} represents the next frequency in the list.

In the next step, the algorithm identify an optimal common line based on the estimated propagation-constant γ_{est}. The common line can change in between different frequency ranges. The identified optimal common line in the specified frequency range has the minimum phase difference from other lines. As the first estimation, Thru standard is chosen as the common line and effective phase differences ϕ_{eff} are identified with length differences Δl between other line standards.

$$\phi_{eff} = sin^{-1}\frac{|e^{-\gamma_{est}\Delta l} - e^{+\gamma_{est}\Delta l}|}{2} \tag{4.6}$$

Shown in Fig. 4.3(a) is the effective phase difference between the designed lines and *Thru* standard. *Line1* covers the frequency band between 3 GHz and 26 GHz with no less than $|20|^\circ$ of phase margin which is commonly accepted as the lowest reliable boundary for TRL. Two additional lines *Line2* and *Line3* were used to extend the lower frequency band down to 0.5 GHz. Two crossover frequencies, 2 GHz and 7 GHz are marked as the upper frequency limits for *Line2* and *Line3* respectively. Still, even at these extremes, each adjacent line exhibits more than 40° of phase margin which is reasonably far from the lowest reliable boundary.

Using multiple lines with the conventional TRL method requires segmenting the band that creates discontinuities in the solution. The Multiline method, however, uses all the lines simultaneously and reduces the error by the use of redundant measurements [4]. As a prevailing indicator of calibration quality, Fig 4.3 (b) shows the calculated normalized standard deviation (NSD). NSD equals one when the conventional TRL method is applied with a quarter-wave line. The accuracy of the method, therefore, increases as NSD gets close to one where obtaining an NSD less than one is possible in the case of using multiple lines. The regions marked with red in Fig. 4.3(b) show the

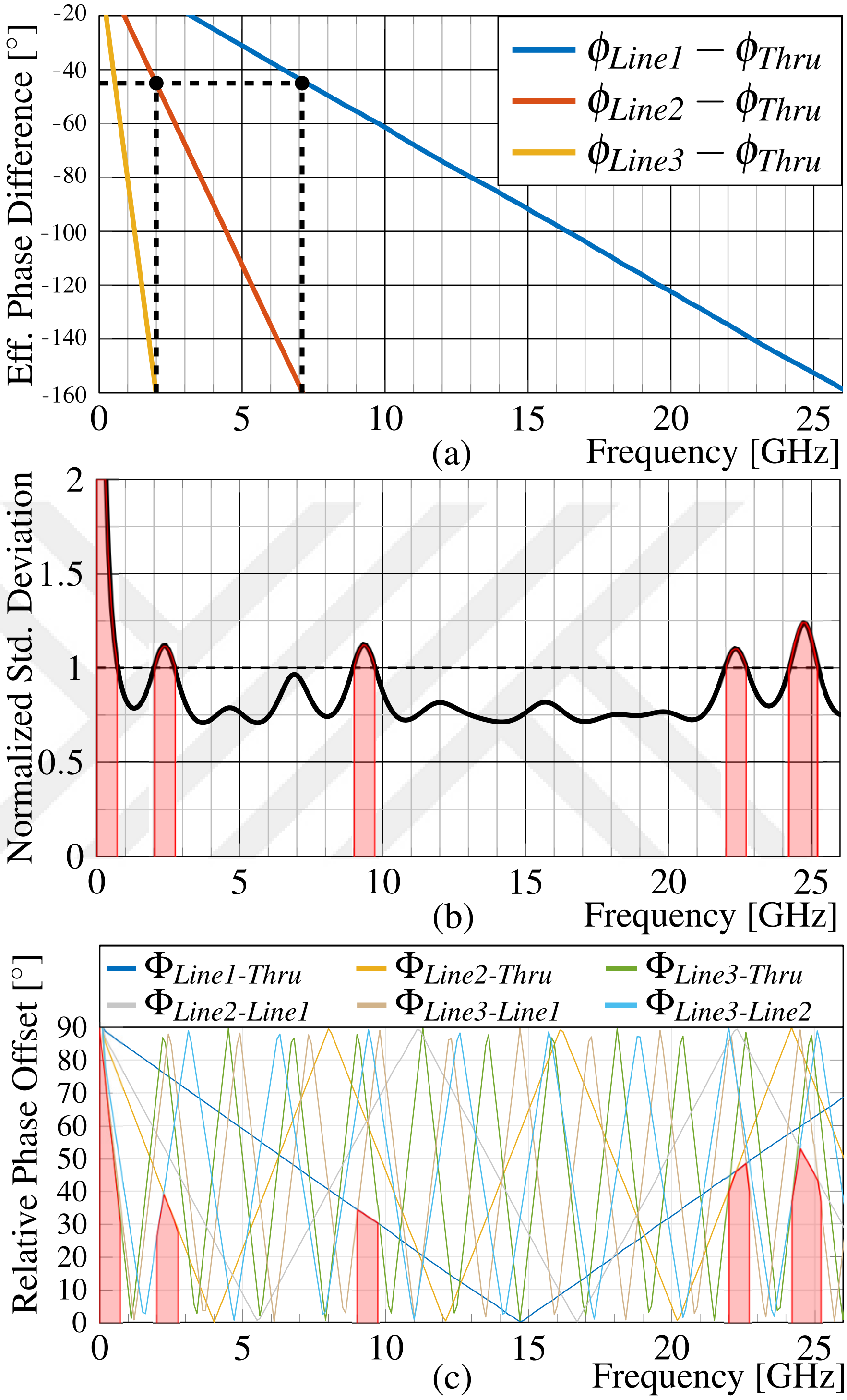

Figure 4.3 : (a) Effective phase difference of *Line1*, *Line2* and *Line3* relative to *Thru* (b) Normalized standard deviation of Multiline TRL calibration (c) Relative phase offset of all line pairs.

frequencies where NSD exceeds one. This is because the lengths of the line standards were calculated for conventional TRL. Same result can also be inferred using Fig. 4.3(c). Defining relative phase offset Φ_{i-j} of calibration standards i and j using

$$\Phi_{i-j} = \left| \left[\phi_j - \phi_i \pmod{\pi} \right] - \frac{\pi}{2} \right| \tag{4.7}$$

simply describes how far the effective phase difference of the line pairs is away from the optimum. The red regions indicate that Φ_{i-j} is greater than 30° where NSD exceeds one.

A comparison of NSDs obtained with each *line-Thru* pair is given in Fig. 4.4(a). They reach their minimum (which is equal to one) when the effective phase difference between line pairs is 90°, whereas the peaks are observed when the effective phase difference between the same pairs is 180°. These peaks never reach to infinity due to the lossy nature of the line and the value of the peaks decreases as the losses increase with frequency. The effect of the peaks where the errors are maximized can be observed on the reflection coefficient of *DUT* after it is de-embedded from its fixtures as shown in Fig. 4.4(b). Omitting the near-DC region and comparing the NSDs of Fig. 4.3(b) and Fig. 4.4(a), the quality of calibration performed with the Multiline method is quite acceptable since NSD in Fig. 4.3(b) is still pretty close to one in the red regions, thereby it has practically no effect on *DUT* reflection coefficient.

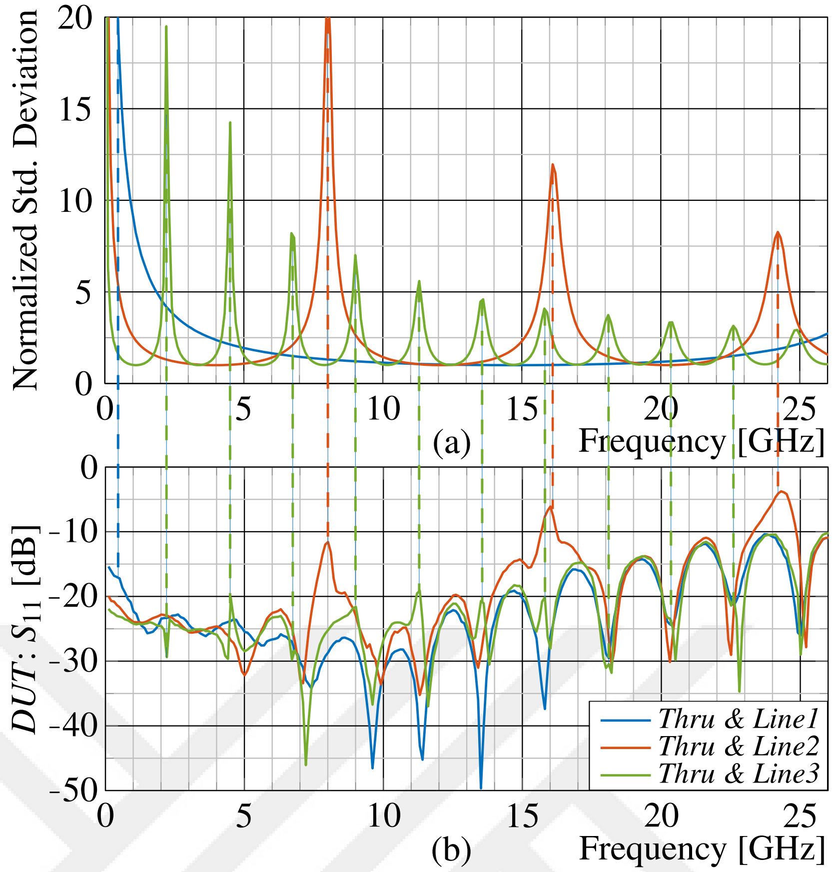

Figure 4.4 : a) Normalized standard deviation obtained with single *line-Thru* pairs. (b) *DUT* return loss after de-embedding with each *line-Thru* pair.

The algorithm solves the eigenvalues in Eq. 4.3 using the selected line pairs for each frequency point. An estimated propagation constant is derived based on the obtained eigenvalues. To assign correct eigenvalues to $e^{\pm\gamma\Delta l}$, the algorithm makes an assignment by choosing one of the roots and calculating the propagation constant. Then compare the calculated value with γ_{est} computed in Eq. 4.4. The same operation is performed for the other root as well and the one which has the minimum difference is selected. The best unbiased linear estimation of γ between the line pairs is based on the Gauss-Markov theorem [19]. The propagation constant, γ, derived by the algorithm is represented in Fig. 4.10. Effective permittivity ε_{eff} is calculated with the Eq. 4.8 and output with respect to frequency are illustrated in Fig. 4.6.

$$\varepsilon_{eff} = -\left[\frac{\gamma}{w/100c}\right] \tag{4.8}$$

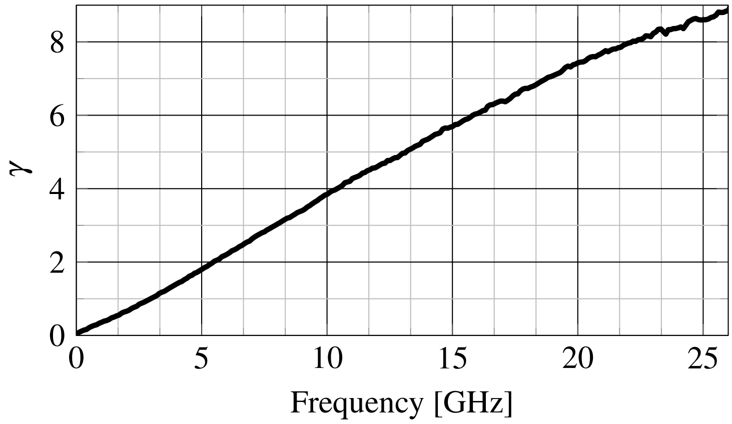

Figure 4.5 : Propagation constant vs Frequency

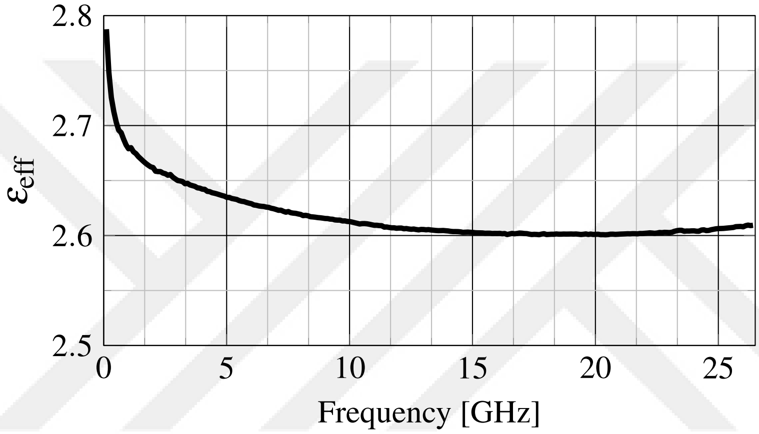

Figure 4.6 : Effective permittivity vs Frequency

Multiline calibration operates by correcting S-parameters relative to the characteristic impedance Z_0 of specified transmission line standards. The method can generate corrected S-parameters without knowing Z_0, but only applicable for waveguides that have similar characteristics. However, once Z_0 of the standards is known, the calibration algorithm can convert the correction coefficients to any desired reference impedance Z_{ref}.

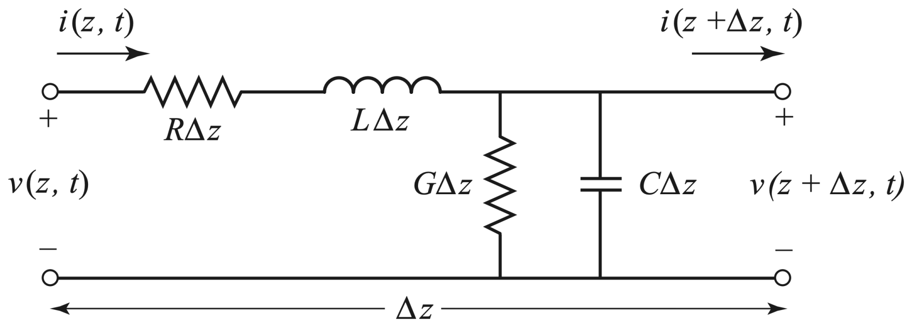

Figure 4.7 : Lumped-element equivalent circuit model of a transmission line [1]

Fig. 4.7 shows an RLGC lumped-element transmission line model characterized by a series impedance R + jwL and a shunt admittance G + jwC where R is the resistance, L the inductance, G the conductance, and C the capacitance. From the transmission line equations given in [20]

$$Z_0 = \sqrt{\frac{R + jwL}{G + jwC}} \tag{4.9}$$

$$\gamma = \sqrt{(R + jwL)(G + jwC)} \tag{4.10}$$

$$Z_0 = \frac{\gamma}{G + jwC} \approx \frac{\gamma}{jwC} \tag{4.11}$$

The characteristic impedance Z_0, expressed in Eq.4.11, is a function dependent on capacitance C and the propagation constant γ. The propagation constant is already calculated by NIST mTRL.

Ignoring the dielectric conductance in CPWs and assuming the capacitance per unit length is not a strong function of the frequency, the capacitance is found using [21]

$$C = Re\left[\frac{1}{jw}\frac{\gamma}{R_{load_{DC}}}\frac{1 + \Gamma_{load}}{1 - \Gamma_{load}}\right] \tag{4.12}$$

where $R_{load_{DC}}$ is the DC resistance of *Load* in Fig. 3.1 with mark "G" which was measured with a simple multimeter. Γ_L is the reflection coefficient of *Load*, after being de-embedded from its fixture. With these findings in hand, the capacitance in Eq. (4.12) was read 1.08 pF/cm near DC as shown in Fig.4.8.

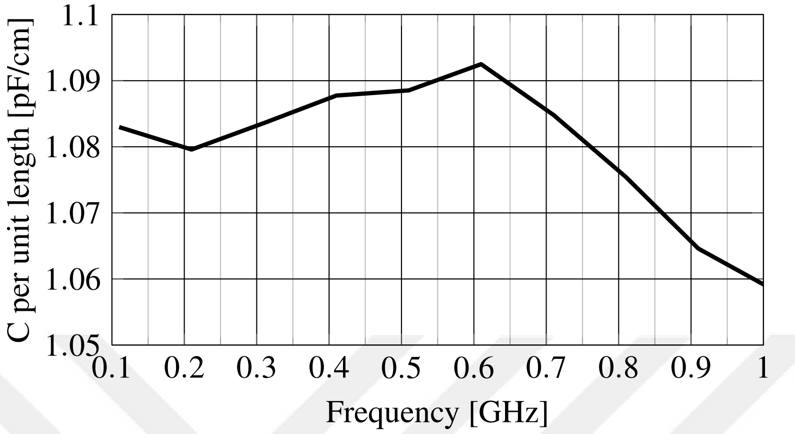

Figure 4.8 : Capacitance per unit length change near DC

The characteristic impedance Z_0, obtained using the capacitance and γ as specified in the Eq. 4.11, is presented in Fig.4.9, indicating that the characteristic impedance is already 50 Ohms.

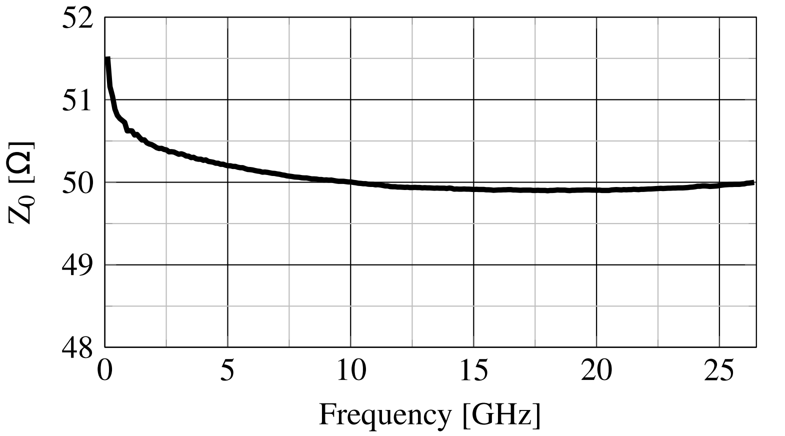

Figure 4.9 : Characteristic impedance vs Frequency

Once the unit capacitance and the reference impedance to be transformed (50 Ω) is provided, another de-embedding routine with impedance transform has been performed on *FDF*. Three results, namely the "Measured" (*FDF*), "Corrected" (*DUT* without impedance transform) and “Renormalized” (*DUT* with impedance transform) have been compared in terms of reflection and transmission coefficients as given in Fig. 4.10 (a) and (b) respectively. The near-identical outputs of “Corrected” and “Renormalized” results reveal that the characteristic impedance of the fabricated lines is quite close to 50 Ω.

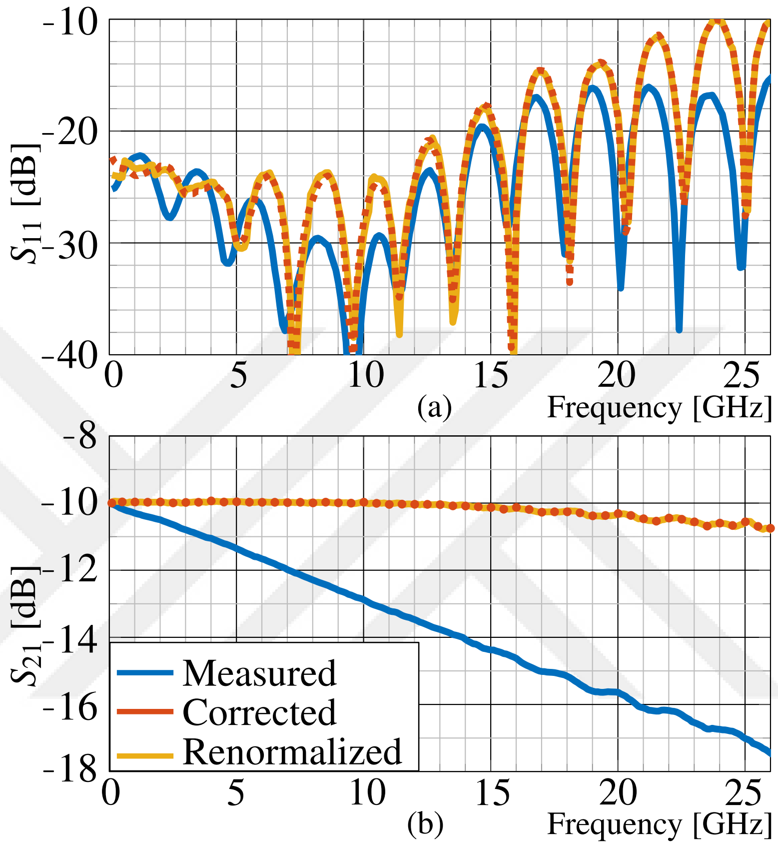

Figure 4.10 : Measurement and de-embedding comparison of *DUT* in terms of (a) Reflection Coefficient (b) Transmission Coefficient.

4.1 Comparison of Reflect Standards

Four different reflection standards were designed for the multiline TRL method. These standards include Direct Open, 38.1mm Open, Direct Short, and 38.1mm short . These configurations are represented by marking as ’B’ and ’C’ in Fig. 3.1. Fig.4.11 (a) illustrates the Smith chart representation for the Direct and 38.1mm Open configurations, while Fig.4.11 (b) demonstrates the Smith chart for the Direct and 38.1mm Short configurations. Both standard types perform true open and short circuit behaviors, starting from the $Z = 0$ and $Z = \infty$ points on the Smith chart. Due to the phase delay dependent on the length of the lines, the turn numbers differ between the standards.

In the calculation of the parameters a_1 and a_2 in Fig.2.2, which are used in the representation of the DUT error box, a reflect standard is employed to resolve the sign ambiguity. The user assigns "-1" for short standards and "+1" for open standards. The comparison is made between the roots found by the algorithm for a_1 and a_2, evaluating how close they are to open or short circuit standards based on user input.

The mTRL de-embedding measurement results obtained with different types and lengths of reflect standards are presented in Fig. 4.12. No noticeable difference was observed with other reflect standards available on the board.

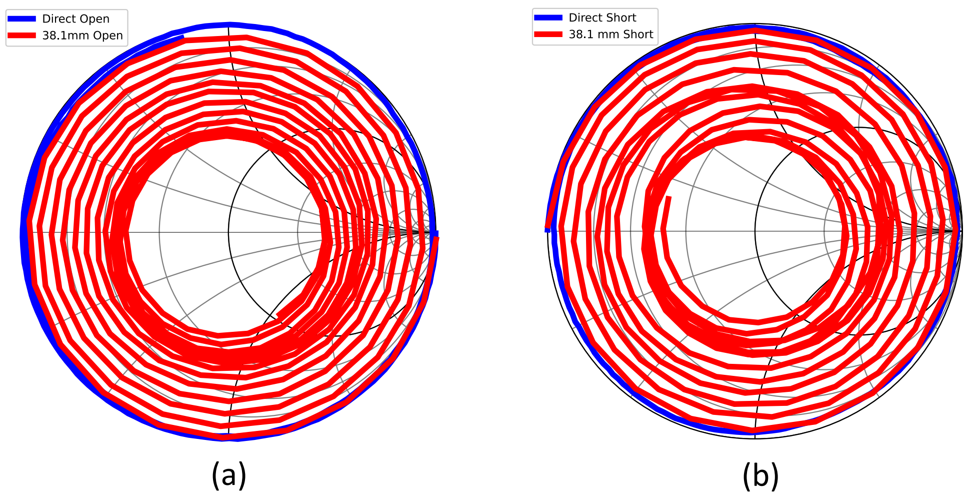

Figure 4.11 : Smith Chart representation of (a) Direct & 38.1mm Open, (b) Direct & 38.1mm Short

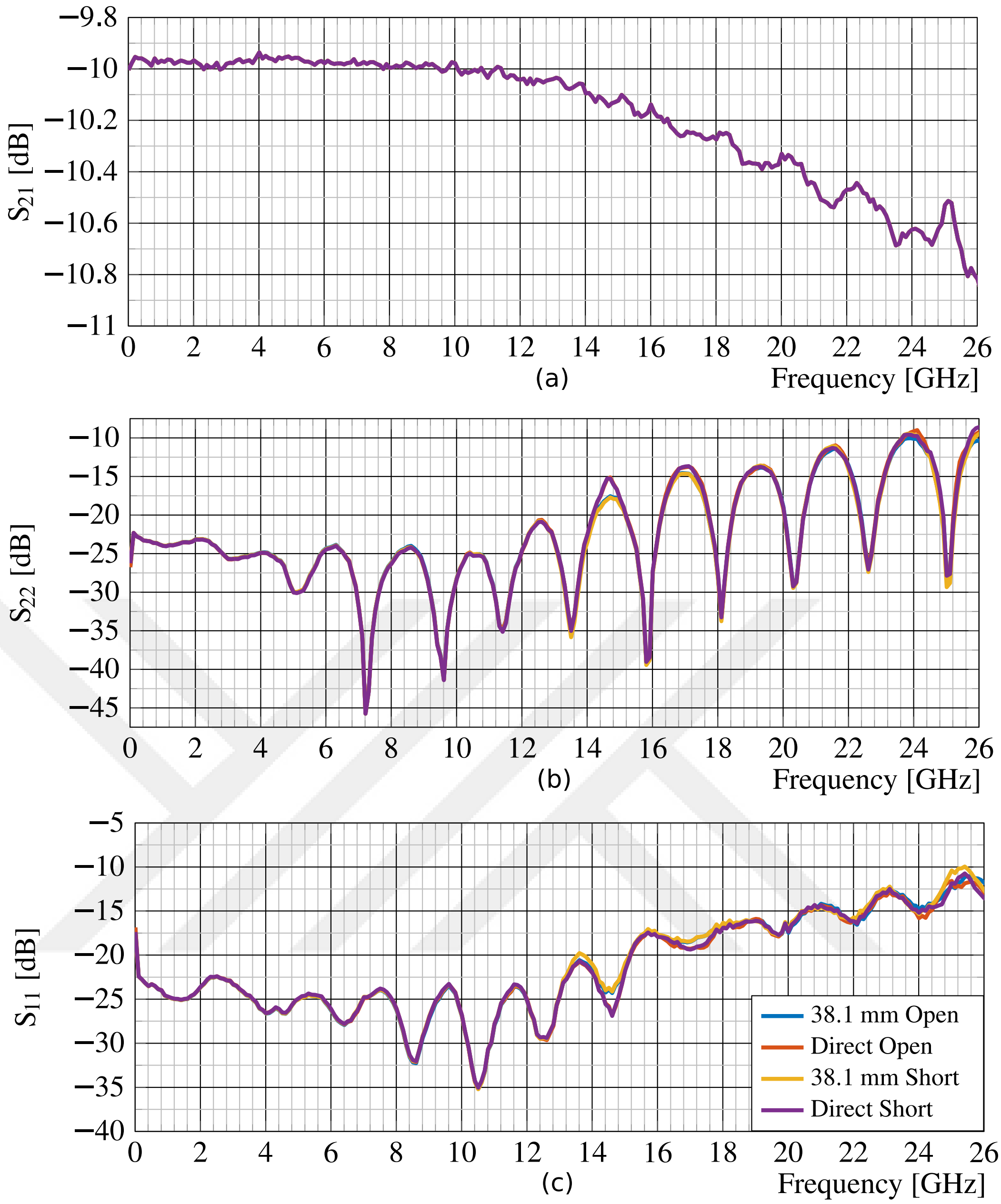

Figure 4.12 : mTRL de-embedding results applied to the Device Under Test (DUT) using reflection standards of Direct, 38.1 mm Open and Short. (a) Transmission Coefficient, S_{21} (b) and (c) Reflection Coefficients, S_{22} and S_{11}.

5. 2X-THRU DE-EMBBEDDING METHOD

Compared to mTRL de-embedding method, the 2X-Thru method simplifies the calibration process, as it requires only a single standard: *Thru*, which is built with cascade connection of two fixtures to be de-embeeded from DUT. Fig.5.1 (a) represents DUT with fixture cascades FDF (Fixture-DUT-Fixture). As demonstrated in Fig. 5.1 (b), the 2X-Thru method is characterized by measuring both sides of test fixtures together. The calibration reference plane is the physical middle point of the 2X-thru standard which divides two identical 1X-fixtures which are FIX-1 and FIX-2.

The de-embedding procedure is by using ABCD scattering parameters, DUT is calculated as follows:

$$DUT = [\mathrm{FIX}_1]^{-1}[\mathrm{FDF}][\mathrm{FIX}_2]^{-1} \tag{5.1}$$

FIX_1 is the fixture model connected to DUT from the left side which is represented as FIX-1; FIX_2 is the fixture model connected to DUT from the right side which is represented as FIX-2 in Fig.5.1. Once the S parameter of 1X-fixtures is obtained, a 2X-thru de-embedding process can be applied to extract the S parameter of DUT from the S parameter of the total structure FDF.

S-parameter calculations of 2X-Thru standard obtained using the three-term error model represented in Fig.5.2 are stated in Eq.5.2 - 5.5. 1X-fixtures are assumed to have equal length and they are uniform.

$$S_{11} = e_{00}^{1} + \frac{(e_{10}^{1})^2 e_{11}^{2}}{1 - e_{11}^{1} e_{11}^{2}} \tag{5.2}$$

$$S_{22} = e_{00}^{2} + \frac{(e_{10}^{2})^2 e_{11}^{1}}{1 - e_{11}^{1} e_{11}^{2}} \tag{5.3}$$

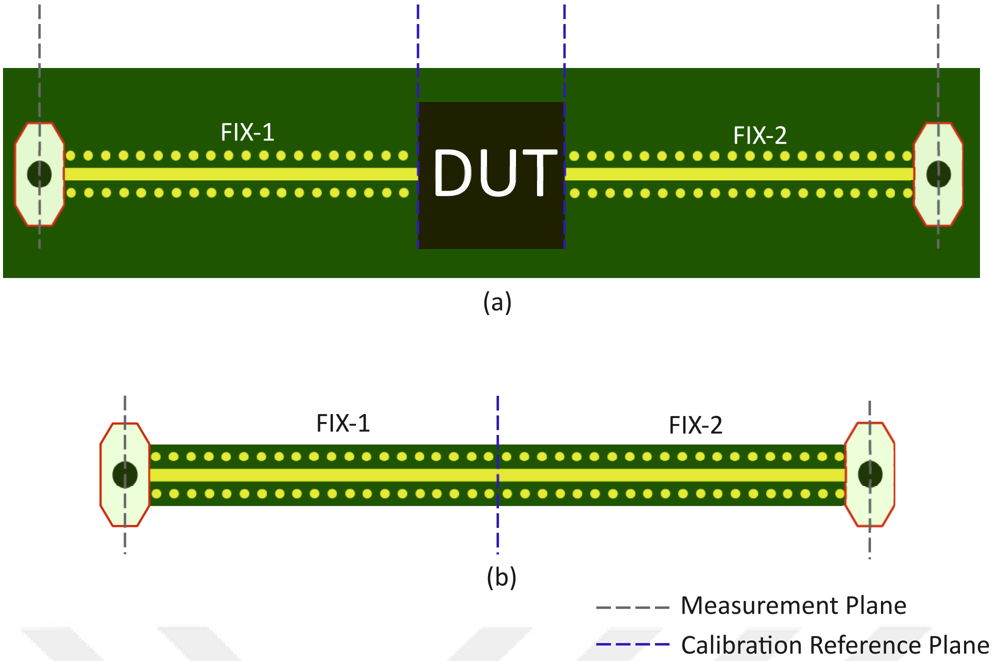

Figure 5.1 : Representation of measurement and calibration reference plane of (a) $FIX_1 - DUT - FIX_2$ and (b) 2X-Thru.

$$S_{21} = \frac{e^1_{10} e^2_{10}}{1 - e^1_{11} e^2_{11}} = \frac{(e^1_{10})^2}{1 - e^1_{11} e^2_{11}} \tag{5.4}$$

$$S_{12} = \frac{e^1_{10} e^2_{10}}{1 - e^1_{11} e^2_{11}} = \frac{(e^2_{10})^2}{1 - e^1_{11} e^2_{11}} \tag{5.5}$$

The e^1_{00} and e^2_{00} directivity terms are derived from time domain information of S_{11} and S_{22} using procedure mentioned in [22].

FIX_1 and FIX_2 fixture models are assumed as symmetric and at that point fixtures models are defined as in Eq.5.6 and Eq.5.7.

$$FIX_1 = \begin{bmatrix} e^1_{00} & e^1_{10} \\ e^1_{10} & e^1_{11} \end{bmatrix} \tag{5.6}$$

$$FIX_2 = \begin{bmatrix} e^2_{00} & e^2_{10} \\ e^2_{10} & e^2_{11} \end{bmatrix} \tag{5.7}$$

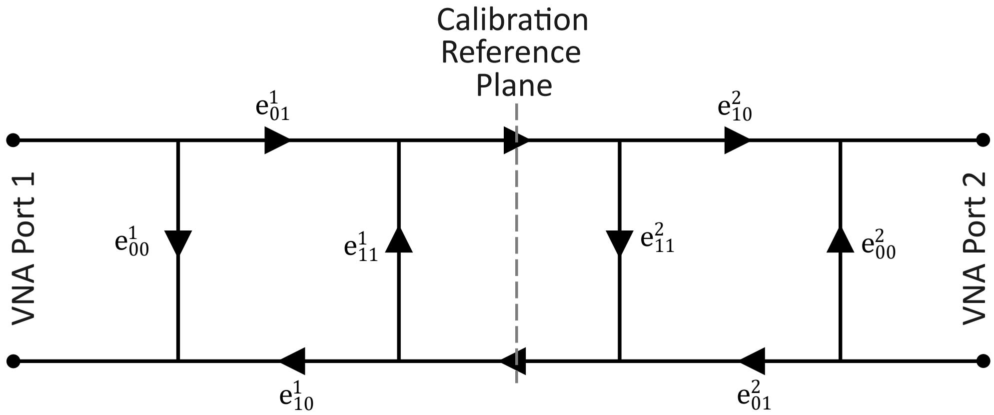

Figure 5.2 : Signal flow a 2X-Thru standard with three term error model representation.

5.1 2x-Thru De-embedding without Impedance Correction

In this section, application and measurement results of 2X-Thru de-embedding method without impedance correction will be explained. Even though there are several commercially available tools which have such a capability, accessing them and verifying calibration accuracy can be difficult. In this thesis, MATLAB® based script provided by IEEE P370 standard [23], and its implementation in "Scikit-rf" with Python programming language [16] have been used to implement the "NZC 2X-Thru without Impedance Correction" algorithm. Scripts are publicly available. IEEE370 standard recommends two methods for de-embedding consistency check [23]. One of them is to analyze the TDR response of (a) fixture, (b) calibration standards, and (c) DUT. Another consistency test is de-embedding of Thru from itself [23]. The maximum acceptable values for residual phase and magnitude are specified in [23]:

- Absolute value of the magnitude of the residual insertion loss < 0.1 dB
- Phase of the self-de-embedded 2X-Thru is < 1 degree

Fig.5.3 represents residual characteristics of Thru after de-embedding from itself and comparison of measured Thru and fixture cascades created by the algorithm. As shown in Fig. 5.3 (a), the magnitude of residual insertion loss remains less than 0.1 dB, and the phase remains in ± 1° across the entire frequency range. Tranmission and insertion

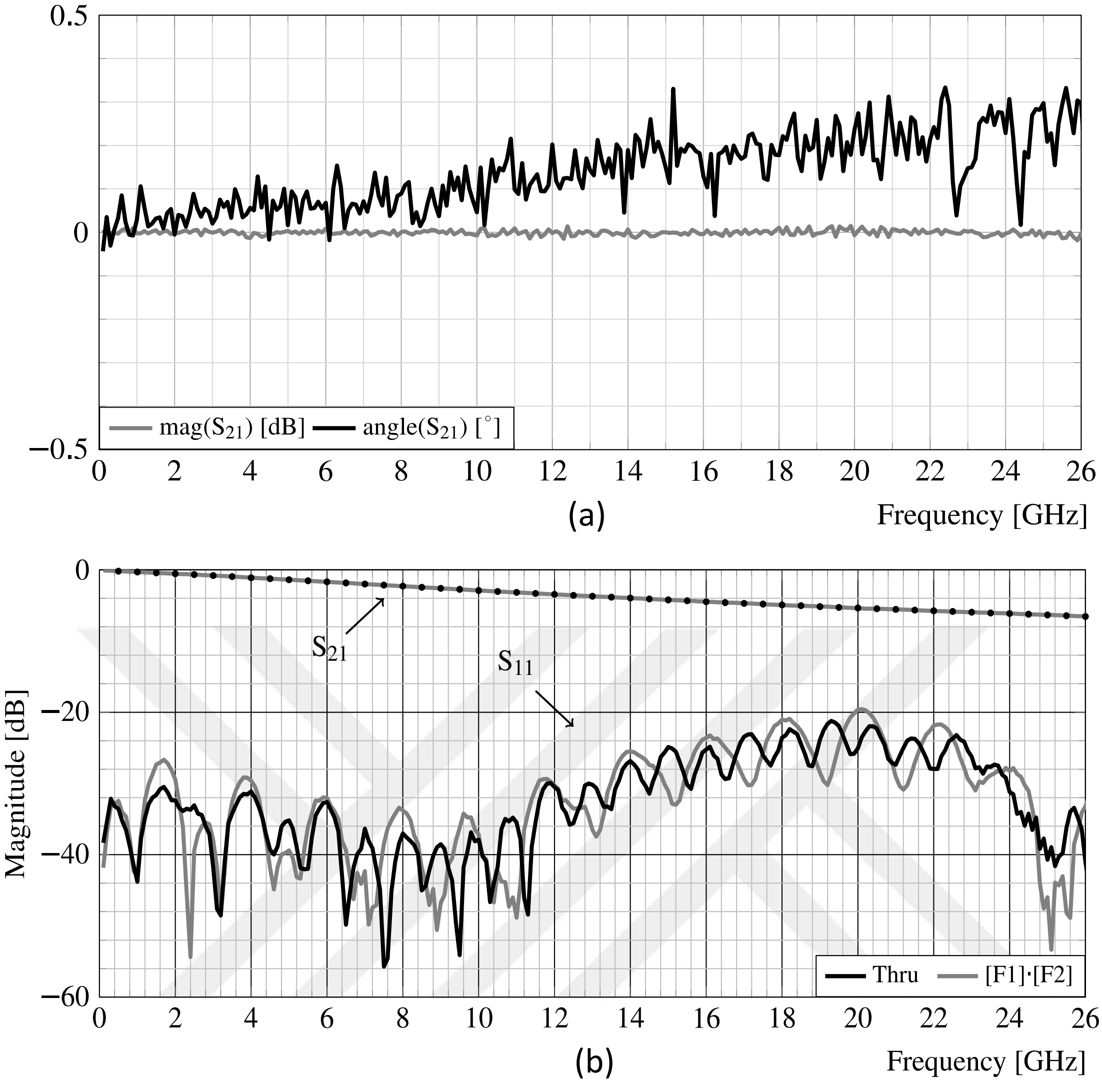

Figure 5.3 : (a) Residual characteristics of Thru after de-embedded from itself. (b) Thru vs. fixture cascades comparison.

loss comparison of Thru and cascaded fixtures are nearly identical, as shared in Fig. 5.3 (b).

5.2 2x-Thru De-embedding with Impedance Correction

Impedance differences between DUT and calibration standards are undesirable, but they may arise due to variations in the manufacturing process or if they are not constructed on the same board. Manufacturing-based variations between the “fixtures” of DUT and Thru, non-causal effects are noticed in the TDR response of DUT resulting in inaccurate de-embedding results [24]. This problem is solved with another technique called impedance correction. This technique is also embedded in Python within “Scikit-rf” library as “ZC Impedance-Corrected 2X-Thru. Algorithm was developed from MATLAB® based script provided by IEEE P370 standard [23]. This scripts are also publicly available and use peeling technique which creates a new fixture model by cascading lossy transmission lines and simultaneously subtracting each cascade from FDF. These transmission lines are created by

(a) Calculating the propagation constant information from Thru,

(b) Getting line characteristic impedance from FDF.

The inaccuracy that comes with the mismatch between the fixtures of Thru and FDF is thus eliminated [10]. The method was applied to same measurement data of Thru and FDF in Fig. 3.1 and S-parameters of DUT were calculated by de-embedding FDF from its fixtures. One method to quantify the accuracy of de-embedding is to analyze the TDR response of (a) fixture, (b) calibration standards, and (c) DUT [11] which are given in Fig. 5(a). The TDR response of the fixture agrees with FDF between t=0 and t=0.5 ns. Both are also nearly identical with Thru up to its midpoint which indicates the similarity of fixtures that built Thru and FDF. Although it may seem that the TDR response of DUT (purpletrace) exhibits a mild non-causality due to a little spike at t=-0.5ns, the result is relatively better than the green-trace showing the TDR response of the same DUT obtained using the standard 2x-Thru method without impedance correction labeled as “DUT-nzc” where nzc is an acronym for “No-impedance-correction”. Another consistency test is shown in Fig. 5(b) where Thru is de-embedded from itself [11]. The magnitude of residual insertion loss remains less than 0.1 dB up to 25 GHz whereas the phase remains nearly in $\pm$ 1°

across the entire frequency range. The input reflection coefficient is given in terms of VSWR which exhibits a good match across the band. Considering that the fixtures are created from FDF, not from Thru, the non-idealities observed in residual plots are due to the slight mismatch between the fixtures of FDF and Thru which is still in the acceptable range. Fig. 5(c) verifies this claim where Thru is compared with the cascade combination of created fixture models. Both are well matched to 50Ω where they exhibit identical transmission characteristics across the entire frequency band.

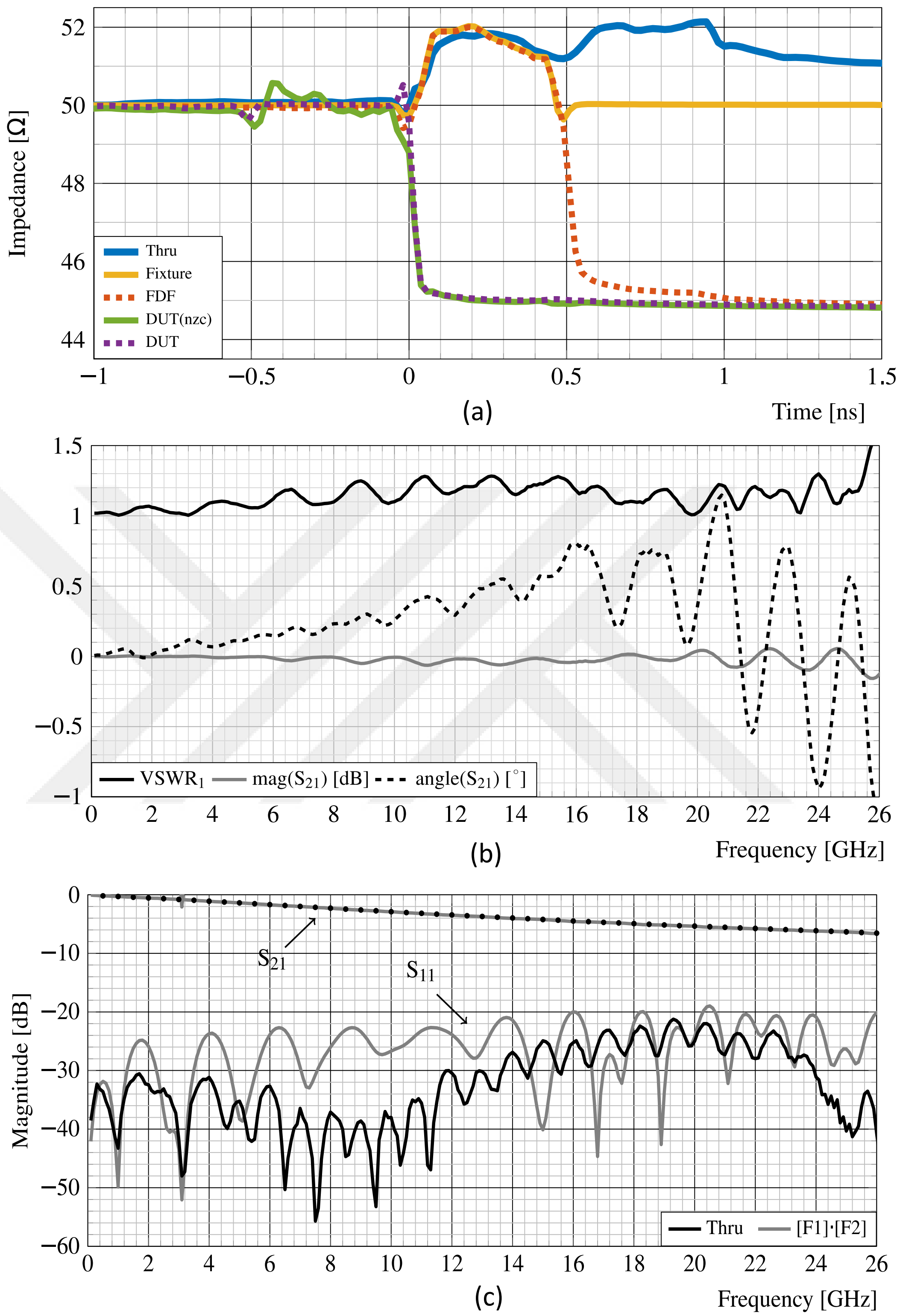

Figure 5.4 : (a) TDR response of calibration standards, fixture and *DUT*. (b) Residual characteristics of *Thru* after being de-embedded from itself (c) *Thru* vs. fixture cascades comparison.

6. COMPARISON OF MEASUREMENT RESULTS

In this chapter, the comparison of results obtained through the previously explained mTRL and 2x-Thru methodologies has been presented. Additionally, to complement these findings, results obtained using commercially available tools have also been included.

In-Situ De-embedding (ISD) is a commercially available tool designed for precise and efficient de-embedding of RF/microwave circuits [9]. The algorithm used in ISD is based on impedance-corrected 2X-Thru. The product meets the highest Class C requirements of IEEE P370. One other commercial de-embedding tool is the AICC De-Embedding Utility, a MATLAB application developed by Amphenol [8]. In addition to ISD, the results obtained using the AICC have also been incorporated into the comparison. This de-embedding tool employs both the 2x-thru and impedance-corrected 2x-thru algorithms.

The transmission, reflection, and TDR results for 10-dB attenuator de-embedding are shared in Fig.6.1. These results are obtained using Python open-source software for mTRL and 2X-Thru, as well as AICC and ISD commercial tools. Up to 20 GHz, all techniques yield comparable results, showing a maximum deviation of 0.1 dB in S_{21}. However, the same is not valid for S_{11} where mTRL exhibits an excessive number of ripples. 2X-Thru results obtained from Python and AICC follow the same pattern for S_{11}. On the other hand, results obtained with ISD have a smoother pattern resembling the average of the other two outcomes. For further analysis, the TDR responses of *DUT* are plotted and compared with other methods as can be seen in Fig. 6.1(c). The comparison indicates that the TDR response of the DUT shows non-causality with the mTRL method, attributed to the impedance variation between calibration standards [9].

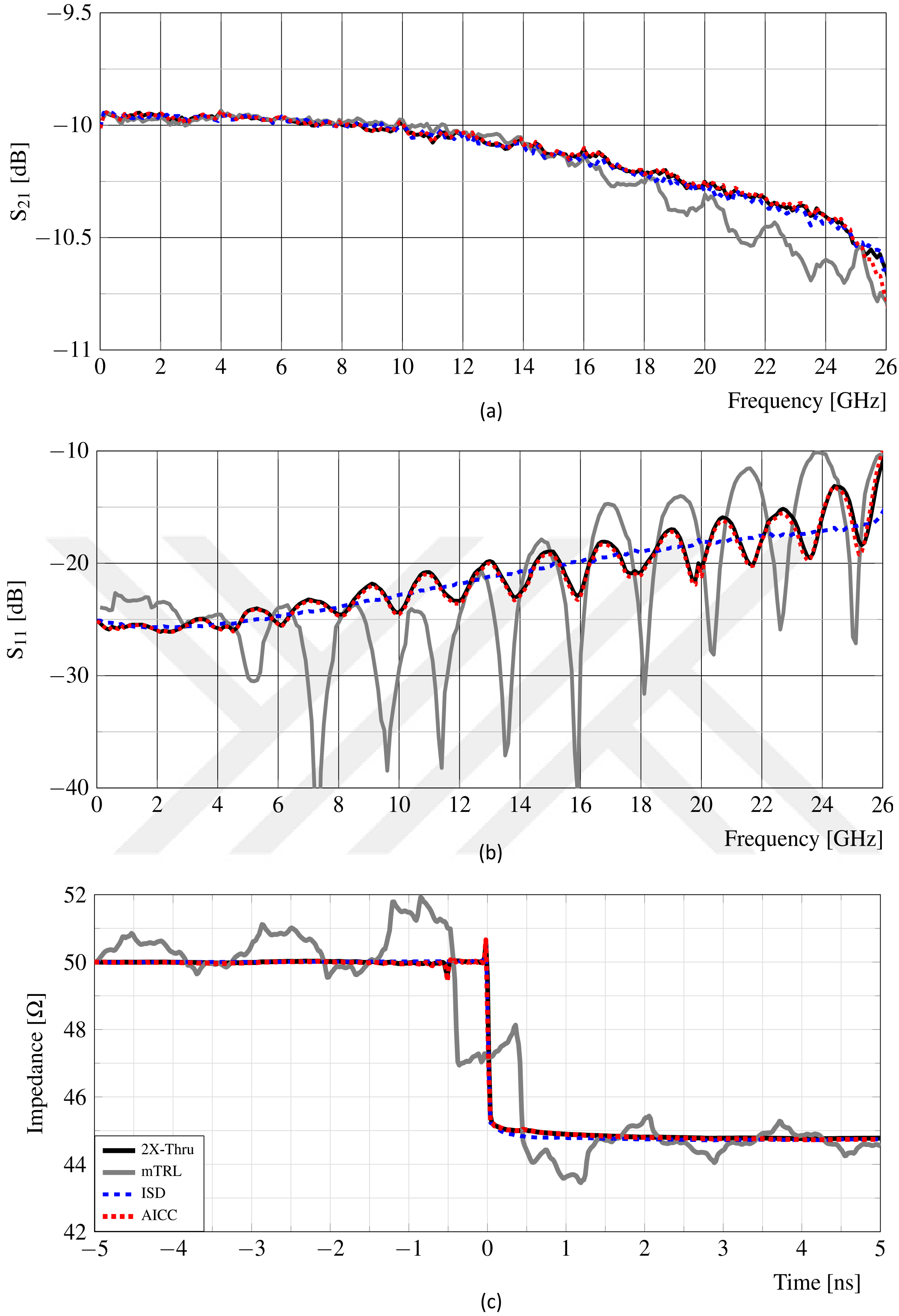

Figure 6.1 : De-embedding comparison of the Multiline method (gray) and 2X-Thru method (black) in terms of: (a) *DUT* S_{21} (b) *DUT* S_{11} and (c) *DUT* TDR.

One of the other verification methods stated in [23] is testing calibration with a resonant printed circuit board (PCB) structure, Beatty line. A Beatty line contains a series step discontinuity, which is constructed as shown in Fig. 6.2:

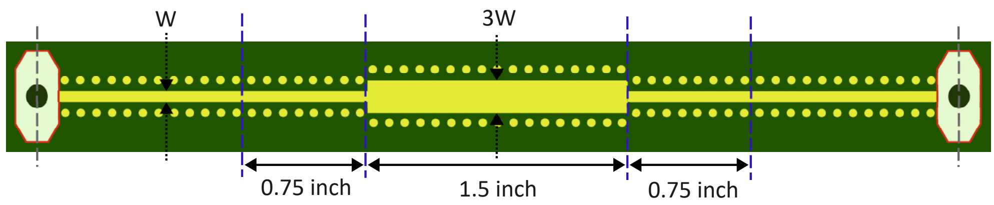

Figure 6.2 : Representation of the Beatty line used in de-embedding verification

A transmission line with a series step discontinuity has been added to the center of the Thru line denoted by A in Fig. 3.1. Designed in compliance with the [23] Beatty standard, the line includes segments of 0.75 lengths on both the right and left sides, each half the length of the 1.5-inch tripled-width discontinuity.

Tripled width results in impedance discontinuity and standing wave resonances. Number of resonance peaks expressed by Eq. 6.1:

$$f = \frac{Nxc}{4L\sqrt{\varepsilon_r}} \tag{6.1}$$

where N is the number of peaks, c is the speed of light, and L is the length of tripled width which is 1.5 inch as shown in Fig. 6.2.

ε_r is the effective dielectric constant (D_k) of the PCB material. D_k of the RO4003C™ laminate is indicated as 3.55 in [25] According to the Eq. 6.1, resonance peak number is 12 up to 26 GHz.

The de-embedding methods presented in this study eliminate the fixture effects and yield sharp resonances as close to the ideal Beatty line behavior. Fig. 6.3 shows a comparison of results obtained from applying mTRL and 2X-Thru de-embedding to the Beatty structure. After the implementation of de-embedding methods, signal resonances have become sharper and fixture effects have been removed as presented in Fig 6.3 (a) transmission and (b) reflection coefficients, respectively.

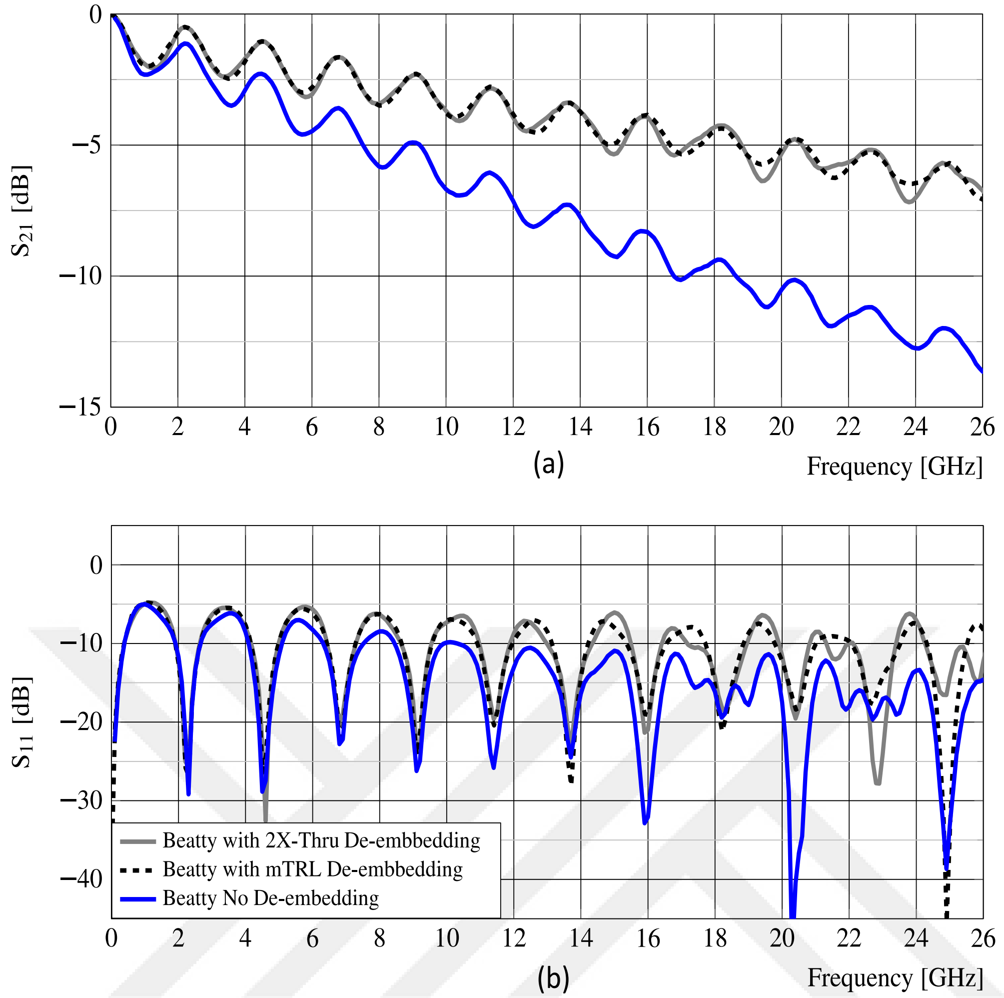

Figure 6.3 : mTRL and 2X-Thru de-embedding comparison of Beatty structure. (a) Reflection Coefficient (b) Transmission Coefficient.

7. GSG BONDWIRE MODEL

The use of bond wires limits the frequency range and degrades the RF performance of the DUT. Bondwire de-embedding is crucial to obtain the actual performance of the DUT. Within the scope of this thesis, a GSG (Ground-Signal-Ground) bond wire model has been developed using both mTRL and 2X-Thru de-embedding methods. The proposed model is characterized up to 26 GHz.

Designed on-wafer thru structure was first measured using RF probes on a probe station, and later, after being bonded to the PCB, it was measured through RF connectors on the PCB. Fig. 7.1 depicts the on-wafer thru structure bonded to the PCB before encapsulation. The on-wafer thru structure has one signal with two ground bonds on each side. The length of the signal bond wire is approximately 750 μm. Fig. 7.2 (b) represents COB of on-wafer thru bonded to the board. Bond wires connect signal and ground pads to the board and signals are routed to the 2.92mm RF connectors. Signal paths were realized using a grounded coplanar waveguide (CPW) with 0.34 mm of line width and 0.13 mm of slot width on a Rogers RO4003C™ laminate with 0.2 mm of dielectric thickness. PCB in Fig. 7.2 (b) contains mTRL and 2X-Thru de-embedding standards implemented for PCB trace de-embedding. A *Thru* was designed with a length twice that of the fixture. An *Open* was implemented as reflect standard. To meet the requirements of the mTRL method, three lines, denoted as *Line1*, *Line2* and *Line3* were also implemented as line standards. Their lengths, relative to the Thru, were defined as Δ_{ℓ_1}=14.5 mm, Δ_{ℓ_2}=6.1 mm, and Δ_{ℓ_3}=3 mm, respectively.

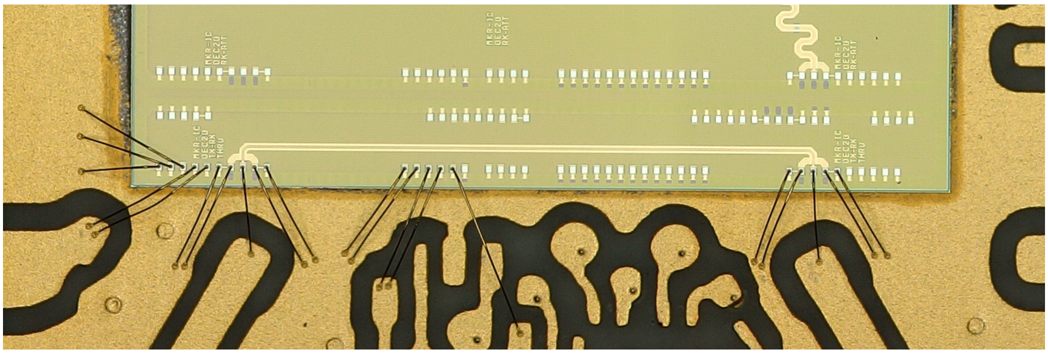

Figure 7.1 : The on-wafer thru structure bonded to the PCB before encapsulation.

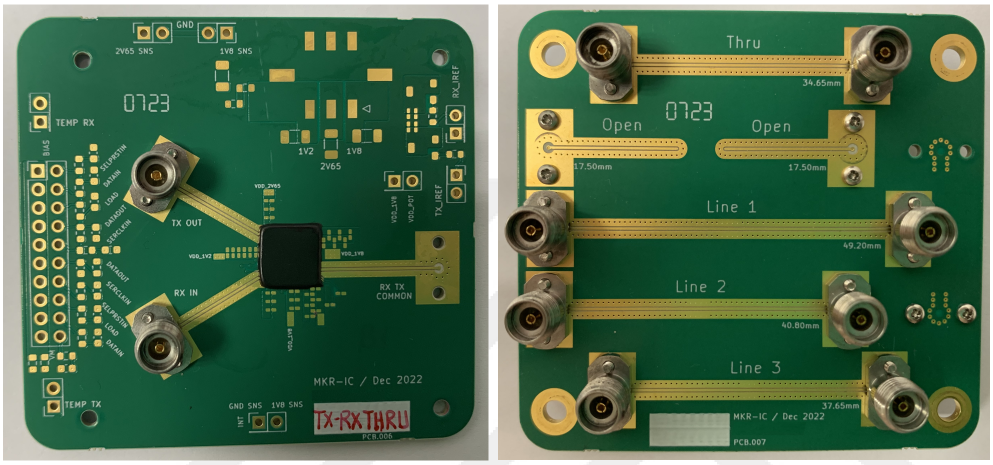

(a) (b)

Figure 7.2 : (a) Chip on Board of the on-wafer thru structure with 2.92mm RF connector outputs. (b) mTRL and 2X-Thru de-embedding structures.

7.1 Extraction of Proposed Model

In this sub-section, the extraction process for the proposed model is outlined, involving the following steps:

1. VNA is calibrated with an E-Cal calibration module to set the reference plane to cable ends which are represented as A and A’ in Fig. 7.3. This procedure is employed as a first-tier calibration.

2. Chip on Board of the on-wafer thru structure in 7.2 (a), mTRL and 2X-Thru calibration standards in Fig. 7.2 (b) are measured.

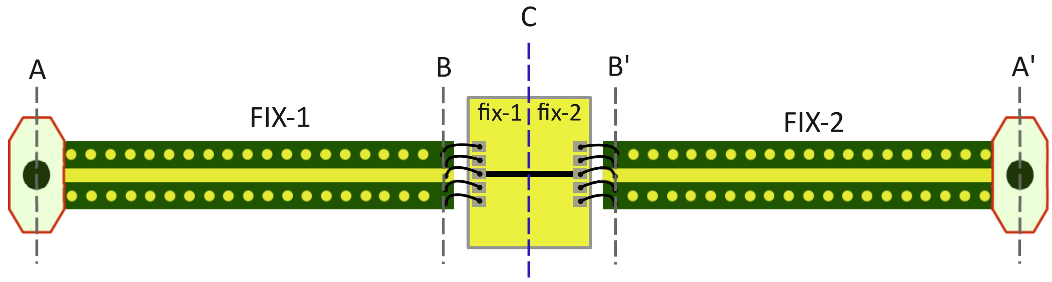

Figure 7.3 : Measurement and calibration reference plane representation of on-wafer thru-die structure with PCB fixtures FIX-1 and FIX-2.

3. mTRL de-embedding algorithm is applied using mTRL standards. The calibration obtained with this method is applied to the Thru standard to eliminate residuals. The calibration plane is extended to the bond wire end, B and B'.

4. The on-wafer thru-die is measured using a suitable GSG RF probe.

5. The 2X-Thru method is applied, and the thru-die model is separated into fix-1 and fix-2 parts.

6. The model obtained with the 2x-Thru method at step 3 is separated into right and left components with respect to the center reference C. One side comprises fix-1 along with the bond wire, represented as [BC], while the other side includes fix-2 and the bond wire, represented as [CB'].

7. One side of the on-wafer thru-die structure, [fix-1] multiplied with the inverse of the [BC] obtained in step 6. GSG bond wire model $[\mathrm{BW}]_{\mathrm{GSG}}$ is represented as :

$$[\mathrm{BW}]_{\mathrm{GSG}} = [\mathrm{BC}]^{-1}[\text{fix-1}] \tag{7.1}$$

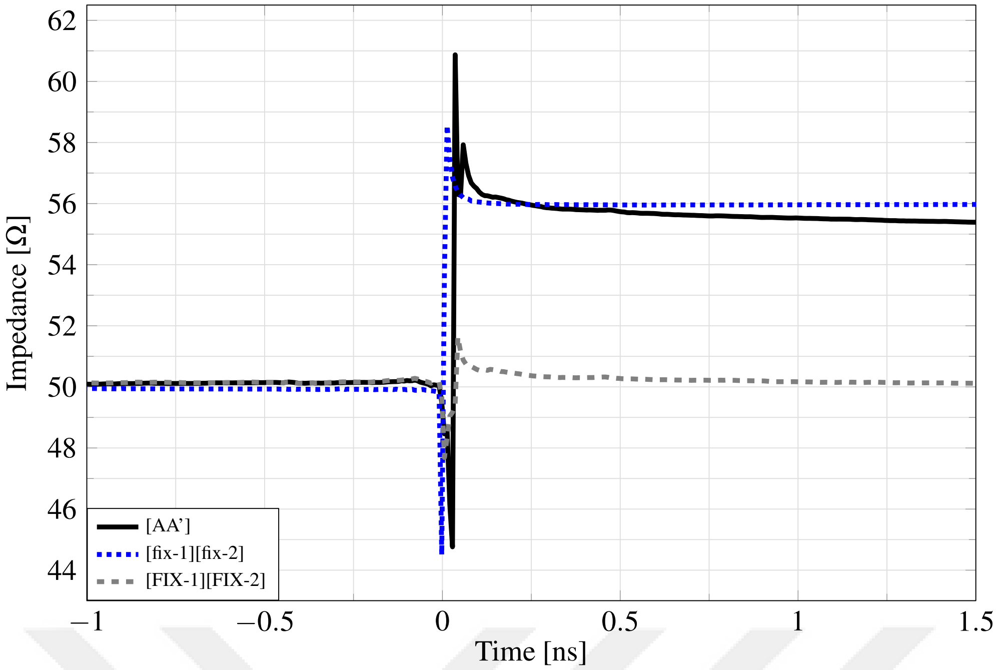

Figure 7.4 : TDR step responses of [AA'], [fix-1][fix-2] and [FIX-1][FIX-2]

TDR responses mentioned as [AA'], [fix-1][fix-2] and [FIX-1][FIX-2] in Fig. 7.4 represents bonded thru-die in Fig. 7.2 (a), the on-wafer thru-die and Thru in Fig. **??** (b), respectively. The TDR response of the [FIX-1][FIX-2] reveals that the impedance of the line remains nearly 50 Ohm, while artifacts in impedance occur at the connector transitions. The bonded thru structure, indicated by the black line, exhibits impedance variations caused by bond wire, as seen in the figure.

To validate the algorithm, measurements of the bond wire with thru-die, and the results were compared by splitting the structure in two and cascading it again. The S_{21} magnitude and phase response of both are presented in Fig. 7.5. Results confirm that when the structure is split into two and cascaded again, the same outcomes can be achieved. Fig. 7.6 (a) is the transmission coefficient of the thru-die structure measured by a GSG probe. The algorithm splits the thru-die into two parts, [fix-1] and [fix-2], by dividing it in half from the center. The transmission response of both sides is presented in Fig. 7.6 (b).

The inverse of the model obtained by splitting the structure in Fig. 7.5 is cascaded with [fix-1] in Fig. 7.6 to obtain the bondwire model. The transmission and reflection coefficients of the obtained bondwire model are shown in Fig. 7.7 (a) and (b).

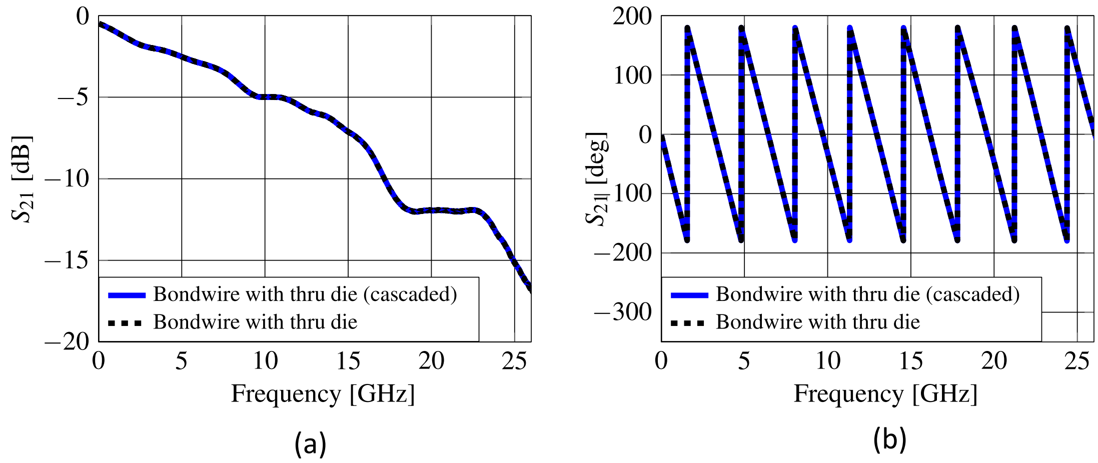

Figure 7.5 : The S_{21} (a) magnitude and (b) phase response comparison of bond wire with thru die and its cascaded version.

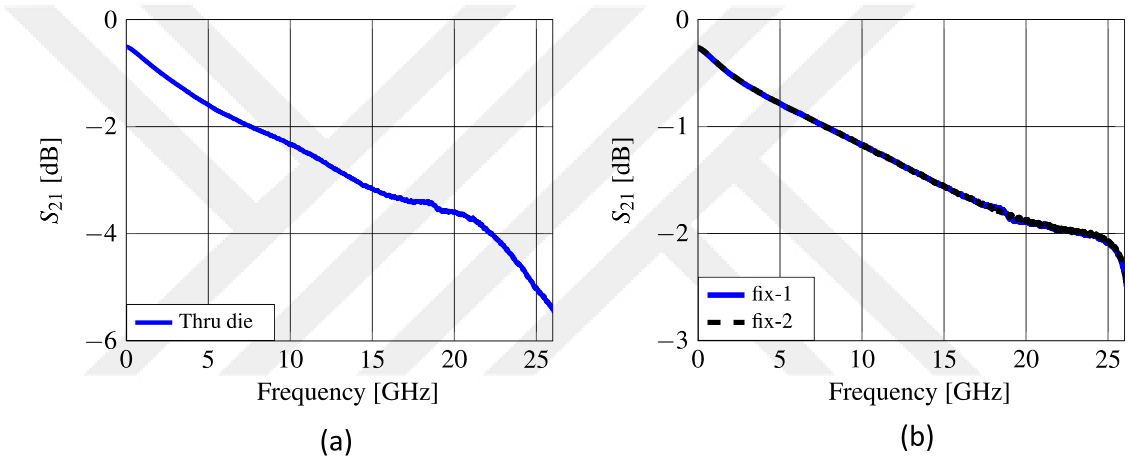

Figure 7.6 : (a) Transmission coefficients of (a) Thru-die structure and (b) [fix-1] and [fix-2] models.

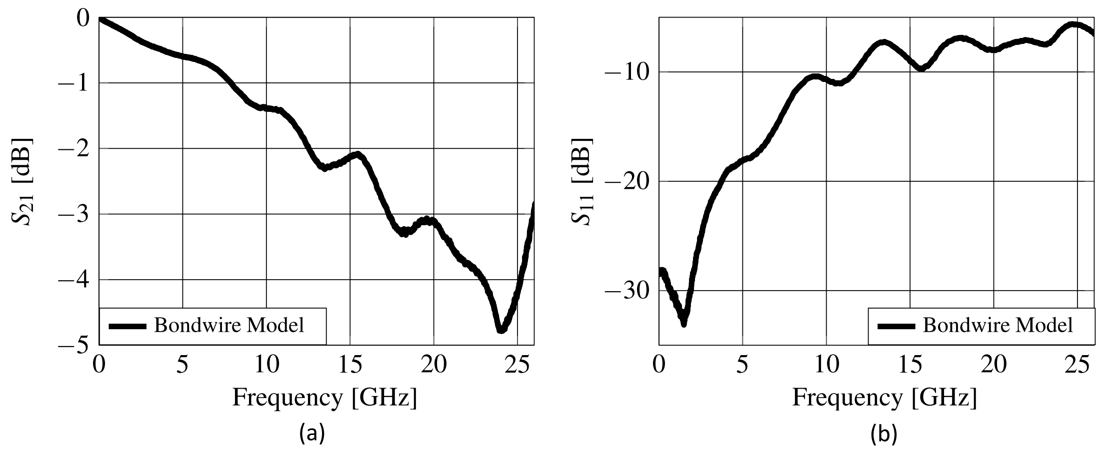

Figure 7.7 : Transmission (a) and reflection (b) coefficients of obtained bond wire model.

7.2 Application of Proposed Model

The application results of the bond wire model obtained in the previous section are shared in this sub-section. In the application of the model, the on-wafer thru structure in Fig. 7.1 has been utilized as the DUT. The transmission and reflection measurement results taken from the DUT on the wafer using probes are presented in Fig. 7.8, marked with red and labeled with the "Die". The die structure on the wafer was diced and bonded onto the PCB in Fig. 7.2 (a). Calibration reference plane is moved to the connectors by performing calibration from cable end via E-cal module. The measurement of the die bonded to the PCB was taken through the RF connectors on the PCB.

The mTRL de-embedding structures in Fig. 7.2 (b) are measured and mTRL process is applied to "Die on PCB" structure in order to move the calibration plane from RF connectors to before the bond wires. De-embedded measurement result of bonded die presented in Fig. 7.8, marked with green, and labeled as "Die on PCB (De-embedded)". Obtained results include on-wafer thru and bond wire cascades.
The obtained bond wire model added to the "Die" measurement result is depicted in black dashed line in Fig. 7.8 (a). The measurement results obtained with mTRL, which include the die and bond wire, and the bond wire fixtures mathematically added to the "Die" results exhibit similar behaviors in transmission and reflection, marked in green and black, respectively.

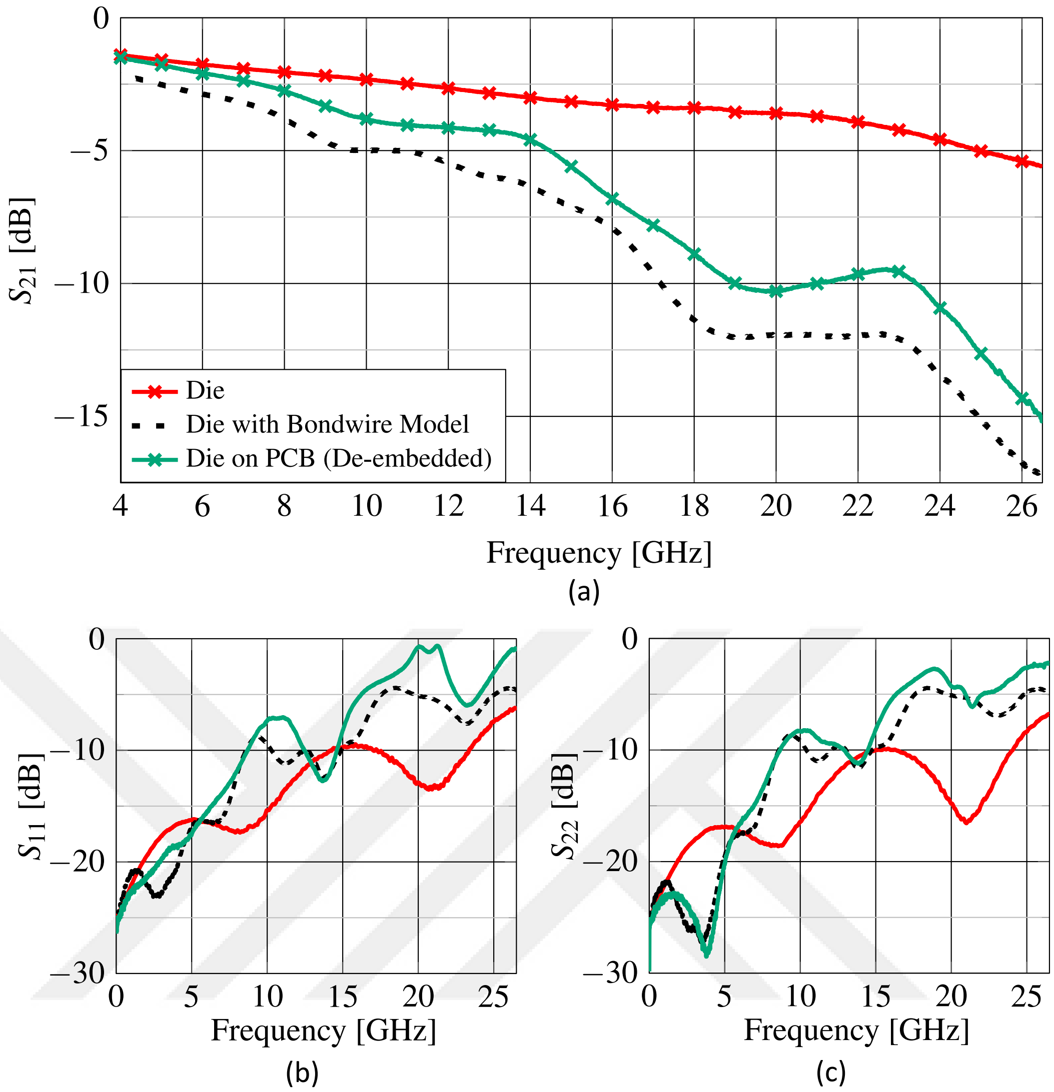

Figure 7.8 : Comparison of the transmission (a) and reflection (b), (c) coefficients of the DUT with applied bond wire model.

8. CONCLUSION

In this thesis, the de-embedding methodologies of Multiline Thru-Reflect-Line (mTRL) and 2X-Thru were systematically investigated using Python open-source software, specifically the "Scikit-rf" library. An individual examination of each method was conducted, focusing on the formulation and implementation details.

The performance comparison between Multiline Thru-Reflect-Line (mTRL) and 2X-Thru methods indicates similar results in terms of transmission and reflection coefficients up to 20 GHz. However, the mTRL method, despite extending the frequency range using multiple standards, introduces complexities, particularly due to impedance variations in the Time Domain Reflectometry (TDR) analysis. This complexity is attributed to differences in the production of calibration standards, leading to impedance variations among them. On the other hand, the 2X-Thru method, requiring only one standard, offers a simpler and cost-effective alternative. This simplicity not only streamlines the de-embedding process but also directly reduces the required Printed Circuit Board (PCB) area, resulting in decreased costs and complexity. The accuracy and efficiency of results obtained using an open-source software implementation of Multiline Thru-Reflect-Line (mTRL) and 2X-Thru have been compared with the results from In-Situ De-embedding (ISD) and AICC De-Embedding Utility which are licensed applications. The transmission coefficients and TDR responses obtained using the 2X-Thru method and licensed tools have similar de-embedding performance results. Finally, a GSG (Ground-Signal-Ground) bond wire model has been developed, utilizing both the Multiline Thru-Reflect-Line (mTRL) and 2X-Thru de-embedding methods. The TDR responses and transmission and reflection coefficients of this obtained bond wire model are comprehensively presented and analyzed. Additionally, the results obtained from applying this model to the DUT are also shared.

In summary, this thesis explored and compared Multiline TRL and 2X-Thru de-embedding methodologies using the "Scikit-rf" library. Results showed similar performance up to 20 GHz, with mTRL introducing complexities due to impedance variations. The 2X-Thru method, requiring one standard, proved a simpler, cost-effective alternative, reducing PCB area and overall complexity. Open-source software results were comparable to licensed tools. Additionally, a GSG bond wire model was developed using both de-embedding methods. This study provides valuable insights into de-embedding approaches, guiding future research and practical applications.

REFERENCES

[1] **Pozar, D.M.** (2005). *Microwave engineering; 3rd ed.*, Wiley, Hoboken, NJ.

[2] **Engen, G. and Hoer, C.** (1979). Thru-Reflect-Line: An Improved Technique for Calibrating the Dual Six-Port Automatic Network Analyzer, *IEEE Transactions on Microwave Theory and Techniques*, *27*(12), 987–993.

[3] **Marks, R. and Phillips, K.** (1989). Wafer-Level ANA Calibrations at NIST, *34th ARFTG Conference Digest*, volume 16, pp.11–25.

[4] **Marks, R.** (1991). A multiline method of network analyzer calibration, *IEEE Transactions on Microwave Theory and Techniques*, *39*(7), 1205–1215.

[5] **Van Hauwermeiren, L.**, **Botte, M. and De Zutter, D.** (1993). A new de-embedding technique for on-board structures applied to the bandwidth measurement of packages, *IEEE Transactions on Components, Hybrids, and Manufacturing Technology*, *16*(3), 300–303.

[6] **Hayden, L.** (2007). A commercial multi-line TRL calibration, *2007 70th ARFTG Microwave Measurement Conference (ARFTG)*, pp.1–6.

[7] **Moon, S.J.**, **Ye, X. and Smith, R.** (2015). Comparison of TRL calibration vs. 2x thru de-embedding methods, *2015 IEEE Symposium on Electromagnetic Compatibility and Signal Integrity*, pp.176–180.

[8] **Amphenol**. *ACS DE-EMBEDDING UTILITY*, https://www.amphenol-cs.com/software.

[9] **Huang, C.** (2016). In-Situ De-embedding, *EDI CON, Beijing, China*.

[10] **Marks, R.B.** (1997). Formulations of the Basic Vector Network Analyzer Error Model including Switch-Terms, *50th ARFTG Conference Digest*, volume 32, pp.115–126.

[11] **Rytting, D.** (1998). Network analyzer error models and calibration methods, *White Paper, September*.

[12] **YAT-10A+ datasheet**. *https://www.minicircuits.com/pdfs/YAT-10A+.pdf*, date retrieved: 21.11.2023.

[13] **IT180A**. *http://www.iteq.com.tw/wp-content/uploads/2017/03/IT-180A-Datasheet.pdf*, date retrieved: 21.11.2023.

[14] **Keysight N7555A**. *https://www.keysight.com/zz/en/product/N7555A/electronic-calibration-module-ecal-dc-26-5-ghz-2-port.html*, date retrieved: 21.11.2023.

[15] **SF1521-60070**. *https://www.svmicrowave.com/Attachment/DownloadFile?downloadId=8677*, date retrieved: 21.11.2023.

[16] **Arsenovic, A.** *et al.* (2022). scikit-rf: An Open Source Python Package for Microwave Network Creation, Analysis, and Calibration [Speaker's Corner], *IEEE Microwave Magazine*, *23*(1), 98–105.

[17] **DeGroot, D.**, **Jargon, J. and Marks, R.** (2002). Multiline TRL revealed, *60th ARFTG Conference Digest, Fall 2002.*, pp.131–155.

[18] **Yau, K.H.K.** (2012). On the Metrology of Nanoscale Silicon Transistors above 100 GHz, `https://api.semanticscholar.org/CorpusID:114042143`.

[19] **Zelen, M.** (1961). *Survey of Numerical Analysis*, McGraw-Hill, New York.

[20] **Brews, J.** (1986). Transmission line models for lossy waveguide interconnections in VLSI, *IEEE Transactions on Electron Devices*, *33*(9), 1356–1365.

[21] **Williams, D. and Marks, R.** (1991). Transmission line capacitance measurement, *IEEE Microwave and Guided Wave Letters*, *1*(9), 243–245.

[22] **Ellison, J.**, **Smith, S.B. and Agili, S.** (2020). Using a 2x-thru standard to achieve accurate de-embedding of measurements, *Microwave and Optical Technology Letters*, *62*(2), 675–682.

[23] (2021). IEEE Standard for Electrical Characterization of Printed Circuit Board and Related Interconnects at Frequencies up to 50 GHz, *IEEE Std 370-2020*, 1–147.

[24] **Ellison, J.J. and Agili, S.S.** (2022). Impedance Corrected De-Embedding, *IEEE Electromagnetic Compatibility Magazine*, *11*(3), 45–48.

[25] **Rogers RO4003C™** . https://www.rogerscorp.com/advanced-electronics-solutions/ro4000-series-laminates/ro4003c-laminates, date retrieved: 21.11.2023.

CURRICULUM VITAE

Name Surname: Tuğçe AYRAÇ

EDUCATION:

- **B.Sc.:** 2019, Istanbul Bilgi University, Engineering Faculty, Electrical and Electronics Engineering Department

PROFESSIONAL EXPERIENCE AND REWARDS:

- 2022 - Present: Test Engineer, Mikroelektronik Ltd. (MKR-IC), Istanbul
- 2019 - 2022: Test and Analysis Engineer, Aselsan, Ankara
- 2019: Completed B.Sc. at Istanbul Bilgi University Electrical and Electronics Engineering Department with high honor ranking 1st in department.

PUBLICATIONS, PRESENTATIONS AND PATENTS ON THE THESIS:

- **T. Ayraç,** A. Özdemirli, E. Apaydın, K. Ozanoglu and M. Yazgı. "Comparative Evaluation of Multiline TRL and 2X-Thru De-Embedding Implementation Methods on Printed Circuit Board Measurements," 2023 19th International Conference on Synthesis, Modeling, Analysis and Simulation Methods and Applications to Circuit Design (SMACD), Funchal, Portugal, 2023

OTHER PUBLICATIONS, PRESENTATIONS AND PATENTS:

- Erdil K., **Ayraç T.**, Akcan Ö. G. and Gökdel Y. D.. (2020) "Piezoresistive disposable weight sensor with increased sensitivity," Turkish Journal of Electrical Engineering and Computer Sciences: Vol. 28: No. 2, Article 27.

- Erdil K., **Ayraç T.**, Akcan Ö. G. and Gökdel Y. D.. "Perforated Paper-Based Piezoresistive Force Sensor," 2019 15th Conference on Ph.D Research in Microelectronics and Electronics (PRIME), Lausanne, Switzerland, 2019, pp. 289-292.

- **Ayraç T.** and Gökdel Y. D.. "A Read-Out System for Disposable Paper-Based Sensors," 2018 3rd International Conference on Computer Science and Engineering (UBMK), Sarajevo, Bosnia and Herzegovina, 2018, pp. 386-389.